

BAYESIAN GEOSTATISTICS USING PREDICTIVE STACKING

LU ZHANG, WENPIN TANG, AND SUDIPTO BANERJEE

ABSTRACT. We develop Bayesian predictive stacking for geostatistical models, where the primary inferential objective is to provide inference on the latent spatial random field and conduct spatial predictions at arbitrary locations. We exploit analytically tractable posterior distributions for regression coefficients of predictors and the realizations of the spatial process conditional upon process parameters. We subsequently combine such inference by stacking these models across the range of values of the hyper-parameters. We devise stacking of means and posterior densities in a manner that is computationally efficient without resorting to iterative algorithms such as Markov chain Monte Carlo (MCMC) and can exploit the benefits of parallel computations. We offer novel theoretical insights into the resulting inference within an infill asymptotic paradigm and through empirical results showing that stacked inference is comparable to full sampling-based Bayesian inference at a significantly lower computational cost.

Keywords. Bayesian inference; Gaussian processes; Geostatistics; stacking.

1. INTRODUCTION

Geostatistics (Cressie, 1993; Chilés and Delfiner, 1999; Zimmerman and Stein, 2010; Banerjee, 2019) refers to the study of a spatially distributed variable of interest, which in theory is defined at every point over a bounded study region of interest. Customary geostatistical modeling proceeds from a latent stochastic process over space that specifies the probability law for the measurements on the variable as a partial realization of the process over a finite set of locations. Inference is sought for the underlying spatial process, which is subsequently used for spatial predictions (Stein, 1999) to grasp the scientific phenomenon under study. The spatial process is often assumed to be stationary and specified by parameters representing the sill, the nugget, the range and, possibly, the smoothness of the process. We collectively refer to these as process parameters that are often empirically estimated from measurements at sampled locations using the “variogram”.

Likelihood-based inference for this process is, however, thwarted by the absence of classical consistent estimators of the process parameters in a customarily preferred infill asymptotic paradigm (see, e.g., Stein, 1999; Zhang, 2004; Zhang and Zimmerman, 2005; Kaufman and Shaby, 2013; Tang et al., 2021). Bayesian inference for geostatistical data (Handcock and Stein, 1993; Berger et al., 2001; Banerjee et al., 2014; Li et al., 2023), while not relying upon asymptotic inference, is also not entirely straightforward. Specifically, irrespective of

how many spatial locations yield measurements, the likelihood fails to mitigate the prior distributions’ impact on the inference. This is undesirable since prior elicitation for the process parameters is challenging. Objective priors for spatial process models have also been pursued, but interpreting such information in practice and their implications in scientific contexts are not uncontroversial. The related question of how effectively (or poorly) the realized data identify these process parameters (in an exact sense from finite samples) has also received commentary (Hodges, 2013; Bose et al., 2018; De Oliveira and Han, 2022).

It is, therefore, not unreasonable to pursue methods that will yield robust inference for the spatial process and for spatial predictions of the outcome at arbitrary points (“kriging”) while circumventing inference on the weakly identified parameters. Instead of seeking families of prior distributions for such parameters, recent efforts at computationally efficient algorithms for geostatistical models have proposed multi-fold cross-validation methods (Finley et al., 2019) to fix the values of weakly identified parameters. However, the metrics for ascertaining optimal values of such parameters are somewhat arbitrary and may not offer robust inference.

Our primary contribution here is to develop and explore Bayesian predictive stacking of geostatistical models. Stacking is a model averaging procedure for generating predictions (Wolpert, 1992; Breiman, 1996; Clyde and Iversen, 2013). Stacking methods and algorithms in diverse data analytic applications are rapidly evolving and a comprehensive review is beyond the scope of this manuscript. Significant developments of stacking methodology in Bayesian analysis have been achieved in recent years (Le and Clarke, 2017; Yao et al., 2018, 2020, 2021), but, to the best of our knowledge, developments in the context of spatial data analysis are lacking. Stacking can be regarded as an alternative to Bayesian model averaging (Madigan et al., 1996; Hoeting et al., 1999). Assume that there are G candidate models $\mathbb{M} = \{\mathcal{M}_1, \dots, \mathcal{M}_G\}$ and each model \mathcal{M}_g is indexed according to a set of fixed values of certain spatial covariance parameters so that the exact posterior distribution is analytically tractable (Section 2). We follow a specific formulation of a spatial hierarchical linear model that seamlessly evinces the familiar closed-form posterior distributions of regression coefficients, random effects and the spatial variance component. The nugget, too, is available in closed form while stacking over all other intractable parameters.

The inferential properties of conventional stacking are largely available for exchangeable models that do not apply to geostatistics. Therefore, we offer theoretical insights within an infill asymptotic paradigm by exploiting tractability offered by the Matérn covariance kernel and conjugate Bayesian linear regression (Section 3). Section 4 offers implementation details, including two algorithms: (i) stacking of means, which combines posterior predictive means; and (ii) stacking of posterior predictive densities (Yao et al., 2018), which combines posterior predictive densities. These methods are evaluated theoretically and empirically through simulation experiments (Section 5) demonstrating that stacked inference is comparable to full Bayesian inference using MCMC at significantly less computational expense.

An illustrative data analysis is presented in Section 6 including comparisons with machine learning interpolation. Section 7 concludes with pointers to future research.

2. BAYESIAN SPATIAL MODELS AND STACKING ALGORITHMS

Let $y(s)$ be a spatially indexed outcome at location $s \in \mathcal{D} \subset \mathbb{R}^d$ and $x(s)$ is a $p \times 1$ vector of predictors observed at s . A customary geostatistical model is

$$y(s) = x(s)^\top \beta + z(s) + \varepsilon(s), \quad (2.1)$$

where β is the $p \times 1$ vector of slopes, $z(s) \sim \text{GP}(0, \sigma^2 R_\Phi(\cdot, \cdot))$ is a zero-centered spatial Gaussian process on \mathbb{R}^d with spatial correlation function $R_\Phi(\cdot, \cdot)$ indexed by parameters Φ , σ^2 is the spatial variance parameter (“partial sill”) and $\varepsilon(s) \sim \mathcal{N}(0, \tau^2)$ is a white noise process with variance τ^2 (“nugget”) capturing measurement error. Processes $z(\cdot)$ and $\varepsilon(\cdot)$ are assumed to be independent. Let $\chi = \{s_1, \dots, s_n\} \in \mathcal{D}$ be a set of n spatial locations yielding measurements $y = (y(s_1), \dots, y(s_n))^\top$ with known values of predictors at these locations collected in the $n \times p$ full rank matrix $X = (x(s_1), \dots, x(s_n))^\top$. We use $y(\chi)$ and y interchangeably while recognizing its dependence on χ . We let $z = (z(s_1), \dots, z(s_n))^\top$ denote the realization of $z(s)$ over χ and let $R_\Phi(\chi) = (R_\Phi(s_i, s_j))_{1 \leq i, j \leq n}$ be the $n \times n$ spatial correlation matrix constructed from the correlation function.

2.1. Conjugate Bayesian spatial model. We extend (2.1) to a conjugate Bayesian hierarchical spatial model,

$$\begin{aligned} y | z, \beta, \sigma^2 &\sim \mathcal{N}(X\beta + z, \delta^2 \sigma^2 I_n), & z | \sigma^2 &\sim \mathcal{N}(0, \sigma^2 R_\Phi(\chi)), \\ \beta | \sigma^2 &\sim \mathcal{N}(\mu_\beta, \sigma^2 V_\beta), & \sigma^2 &\sim \text{IG}(a_\sigma, b_\sigma), \end{aligned} \quad (2.2)$$

where we fix Φ , the noise-to-spatial variance ratio $\delta^2 := \frac{\tau^2}{\sigma^2}$, and $\mu_\beta, V_\beta, a_\sigma$, and b_σ are fixed hyper-parameters specifying the prior distributions for β and σ^2 . Posterior distributions are summarized in the following lemma (also see Kitanidis, 1986; Handcock and Stein, 1993; Gaudard et al., 1999; Banerjee, 2020, for exact Bayesian inference).

Lemma 2.1. *Let $\gamma = (\beta^\top, z^\top)^\top$. The posterior distribution of (γ, σ^2) from (2.2) is*

$$p(\gamma, \sigma^2 | y, \Phi, \delta^2) = \underbrace{\text{IG}(\sigma^2; a_\sigma^*, b_\sigma^*)}_{p(\sigma^2 | y)} \times \underbrace{\mathcal{N}(\gamma; \hat{\gamma}, \sigma^2 M_*)}_{p(\gamma | \sigma^2, y)}, \quad (2.3)$$

where $\hat{\gamma} = M_* X_*^\top V_*^{-1} y_*$, $y_* = [y, \mu_\beta, 0]^\top$, $a_\sigma^* = a_\sigma + n/2$, $b_\sigma^* = b_\sigma + \frac{1}{2}(y_* - X_* \hat{\gamma})^\top V_*^{-1} (y_* - X_* \hat{\gamma})$,

$$M_*^{-1} = X_*^\top V_*^{-1} X_*, \quad X_*^\top = \begin{bmatrix} X^\top & I_p & 0 \\ I_n & 0 & I_n \end{bmatrix} \quad \text{and} \quad V_* = \begin{bmatrix} \delta^2 I_n & 0 & 0 \\ 0 & V_\beta & 0 \\ 0 & 0 & R_\Phi(\chi) \end{bmatrix}. \quad \text{The posterior}$$

distribution $p(\gamma | y, \Phi, \delta^2)$ is multivariate Student’s t (i.e. $t_{2a_\sigma^*}(\gamma; \hat{\gamma}, (b_\sigma^*/a_\sigma^*)M_*)$) with degrees of freedom $2a_\sigma^*$, location $\hat{\gamma}$ and scale matrix $(b_\sigma^*/a_\sigma^*)M_*$.

Proof. The proof is a straightforward adaptation of familiar results from the Normal-Gamma family of distributions (Kitanidis, 1986; Handcock and Stein, 1993). \square

Furthermore, let $\tilde{\chi} = \{\tilde{s}_1, \dots, \tilde{s}_m\}$ be a set of m unknown points in \mathcal{D} , \tilde{z} and \tilde{y} be the $m \times 1$ vectors with elements $z(\tilde{s}_i)$ and $y(\tilde{s}_i)$ for $i = 1, 2, \dots, m$. Let $\tilde{X} = (x(\tilde{s}_1), \dots, x(\tilde{s}_m))^T$ be the $m \times p$ matrix that carries the values of predictors at $\tilde{\chi}$ and let $J_\Phi(\chi, \tilde{\chi}) = (R_\Phi(s, s'))_{\{s \in \chi, s' \in \tilde{\chi}\}}$. Then, spatial predictive inference follows from the posterior distribution

$$p(\tilde{z}, \tilde{y} | y, \Phi, \delta^2) = \int p(\tilde{y} | \tilde{z}, \beta, \sigma^2, \Phi, \delta^2) p(\tilde{z} | z, \sigma^2, \Phi, \delta^2) p(\gamma, \sigma^2 | y, \Phi, \delta^2) d\gamma d\sigma^2, \quad (2.4)$$

which is again a multivariate t distribution with degrees of freedom $2a_\sigma^*$, location $\tilde{\mu}$ and scale matrix $(b_\sigma^*/a_\sigma^*)\tilde{M}$ where $\tilde{\mu} = W\hat{\gamma}$, $\tilde{M} = WM_*W^T + M_2$, $M_1 = R_\Phi(\tilde{\chi}) - J_\Phi^T(\chi, \tilde{\chi})R_\Phi^{-1}(\chi)J_\Phi(\chi, \tilde{\chi})$, $W = \begin{bmatrix} 0 & J_\Phi^T(\chi, \tilde{\chi})R_\Phi^{-1}(\chi) \\ \tilde{X} & J_\Phi^T(\chi, \tilde{\chi})R_\Phi^{-1}(\chi) \end{bmatrix}$ and $M_2^{-1} = \begin{bmatrix} \frac{1}{\delta^2}I_m + M_1^{-1} & -\frac{1}{\delta^2}I_m \\ -\frac{1}{\delta^2}I_m & \frac{1}{\delta^2}I_m \end{bmatrix}$. Specifically, the predictive distributions $p(z(s_0) | y, \Phi, \delta^2)$ and $p(y(s_0) | y, \Phi, \delta^2)$ are also available in analytic form as non-central t distributions for any single point $s_0 \in \mathcal{D}$. Bayesian inference can proceed from exact posterior samples obtained from (2.3) as follows. We first draw values of $\sigma^2 \sim IG(a_\sigma^*, b_\sigma^*)$ followed by a single draw of $\gamma \sim N(\hat{\gamma}, \sigma^2 M_*)$ for each drawn value of σ^2 . This yields samples $\{\gamma, \sigma^2\}$ from (2.3). Predictive inference for the latent process $z(s_0)$ and the outcome $y(s_0)$ is obtained by sampling from (2.4) by drawing a value of $\tilde{z} \sim N(\mu_z(\gamma), \sigma^2 V_{z|\cdot})$ with $\mu_z(\gamma) := J_\Phi^T(\chi, \tilde{\chi})R_\Phi^{-1}(\chi)z$ and $V_{z|\cdot} := R_\Phi(\tilde{\chi}) - J_\Phi^T(\chi, \tilde{\chi})R_\Phi^{-1}(\chi)J_\Phi(\chi, \tilde{\chi})$ for each value of $\{\gamma, \sigma^2\}$ drawn above (see Section 3.4 in Banerjee (2020)), then drawing a value of $\tilde{y} \sim N(\tilde{X}\beta + \tilde{z}, \sigma^2 \delta^2 I_m)$ for each drawn value of β (extracted from γ), σ^2 and \tilde{z} .

The above tractability is only possible if Φ and δ^2 are fixed. While some learning from data is possible, these parameters are not consistently estimable (Zhang, 2004) and impedes convergence. Diggle and Ribeiro (2007) proposed inference with discrete priors on these parameters (Ribeiro Jr et al., 2007), which still entails evaluating the full conditional densities and can encounter numerical instabilities. Alternate approaches using K -fold cross-validation have been explored with limited success (Finley et al., 2019). We, instead, avoid numerically computing the marginal posterior for the prefixed parameters and opt for optimization based on stacking over a set of fixed values of $\{\Phi, \delta^2\}$.

2.2. Stacking algorithms for Bayesian spatial models. Let $\{\mathcal{M}_g, g = 1, \dots, G\}$ be the set of candidate models. The Bayes predictor for $y(s_0)$ under model \mathcal{M}_g , for each $g = 1, \dots, G$, is $\mathbb{E}_g(y(s_0) | y, \mathcal{M}_g)$, where $\mathbb{E}_g(\cdot | y, \mathcal{M}_g)$ is the expectation with respect to $p(y(s_0) | y, \mathcal{M}_g) = t_{2a_\sigma^*}(y(s_0); h_g^T \hat{\gamma}_g, (b_\sigma^*/a_\sigma^*)h_g^T M_* h_g)$ with $h_g^T = [x^T(s_0), J_{\Phi_g}(s_0, \chi)R_{\Phi_g}^{-1}(\chi)]$ and a_σ^* , b_σ^* , $\hat{\gamma}_g$ and M_* given by Lemma 2.1 with $\Phi = \Phi_g$ and $\delta^2 = \delta_g^2$. Stacking will combine

the G Bayes predictors as a weighted average,

$$\sum_{g=1}^G w_g \mathbb{E}_g(y(s_0) | y) = \sum_{g=1}^G w_g h_g^\top \hat{\gamma}_g, \quad (2.5)$$

where $\{w_1, \dots, w_G\}$ are the stacking weights. We refer to (2.5) as the stacked predictor. Subject to the constraint that stacking weights are non-negative and their sum equals one, we define the corresponding stacked predictive density as $\sum_{g=1}^G w_g p(y(s_0) | y, \mathcal{M}_g)$. We consider two stacking algorithms: stacking of means and stacking of predictive densities.

Stacking of means: This is the most natural stacking algorithm adapted from Breiman (1996). Define the leave-one-out (LOO) Bayes predictor for $y(s_i)$ under model \mathcal{M}_g as $\hat{y}_g(s_i) = \mathbb{E}_g(y(s_i) | y_{-i}, \mathcal{M}_g) = h_{g,-i}^\top \hat{\gamma}_{g,-i}$, where y_{-i} is the data without the i -th observation, $h_{g,-i}^\top$ is defined as in (2.5) but with s_i and $\chi_{-i} = \chi \setminus \{s_i\}$ replacing s_0 and χ , respectively, and $\hat{\gamma}_{g,-i}$ is obtained from Lemma 2.1 applied to the data without s_i . The expectation $\mathbb{E}_g(\cdot | y_{-i}, \mathcal{M}_g)$ is calculated with respect to $p(y(s_i) | y_{-i}, \mathcal{M}_g) = t_{a_{\sigma,-i}^*} \left(y(s_i); h_{g,-i}^\top \hat{\gamma}_{g,-i}, \frac{b_{\sigma,-i}^*}{a_{\sigma,-i}^*} h_{g,-i}^\top M_{*, -i} h_{g,-i} \right)$, where $a_{\sigma,-i}^*$ and $b_{\sigma,-i}^*$ are, again, provided in Lemma 2.1 for the data excluding s_i . Stacking of means determines the optimal weights as

$$\arg \min_w \sum_{i=1}^n \left(y(s_i) - \sum_{g=1}^G w_g \hat{y}_g(s_i) \right)^2. \quad (2.6)$$

Stacking of predictive densities: Following the generalized Bayesian stacking framework in Yao et al. (2018), we devise a second stacking algorithm for spatial analysis, which we refer to as stacking of predictive densities. This algorithm finds the distribution in the convex hull $\mathcal{C} = \{ \sum_{g=1}^G w_g \times p(\cdot | \mathcal{M}_g) : \sum_g w_g = 1, w_g \geq 0 \}$ that is optimal according to some proper scoring functions. Here $p(\cdot | \mathcal{M}_g)$ refers to the distribution of interest under model \mathcal{M}_g . Let $\mathcal{S}_1^G = \{ w \in [0, 1]^G : \sum_{g=1}^G w_g = 1 \}$ and $p_t(\cdot | y)$ be the true posterior predictive distribution. Using the logarithmic score (corresponding to the KL divergence), we seek w so that

$$\max_{w \in \mathcal{S}_1^G} \frac{1}{n} \sum_{i=1}^n \log \left(\sum_{g=1}^G w_g \underbrace{t_{a_{\sigma,-i}^*} \left(y(s_i); h_{g,-i}^\top \hat{\gamma}_{g,-i}, \frac{b_{\sigma,-i}^*}{a_{\sigma,-i}^*} h_{g,-i}^\top M_{*, -i} h_{g,-i} \right)}_{p(y(s_i) | y_{-i}, \mathcal{M}_g)} \right). \quad (2.7)$$

The optimal distribution $\sum_{g=1}^G w_g p(y(s_i) | y_{-i}, \mathcal{M}_g)$ provides a ‘‘likelihood’’ of observing $y(s_i)$ on location s_i given other data. Therefore, $\prod_{i=1}^n \sum_{g=1}^G w_g p(y(s_i) | y_{-i}, \mathcal{M}_g)$ serves as a pseudo-likelihood that measures the performance of prediction based on the weighted average of the LOO predictors for all observed locations.

Stacking using K-fold cross-validation predictors: Solving stacking weights relies upon computing the Bayes predictor and predictive density. Computing the exact LOO

Bayes predictor and predictive densities for all observed locations $\{s_1, \dots, s_n\}$ requires re-fitting a model n times. For a Gaussian latent variable model with the number of parameters larger than the sample size n , there are limited choices for approximating LOO predictors accurately without the onerous computation (see, e.g., Vehtari et al., 2016). Instead of using the LOO predictors, computing predictors through K -fold cross-validation is more practical. Using K -fold cross-validation instead of LOO in stacking is explored in Breiman (1996), who demonstrated that 10-fold cross-validation provides more efficient predictors than LOO. If the data is partitioned into K folds and $y[-k]$ denotes the observed outcomes that are not included in the k -th fold, then, following (2.7), we have $p(y(s_i) | y[-k], \mathcal{M}_g) = t_{a_\sigma^*[-k]} \left(y(s_i); h_g[-k]^T \hat{\gamma}_g[-k], \frac{b_\sigma^*[-k]}{a_\sigma^*[-k]} h_g[-k]^T M_*[-k] h_g[-k] \right)$, where s_i is in k -th folder. Here, $a_\sigma^*[-k]$, $b_\sigma^*[-k]$, $h_g[-k]$, and $M_*[-k]$ correspond to $a_{\sigma,-i}^*$, $b_{\sigma,-i}^*$, $h_{g,-i}$, and $M_{*, -i}$ in $p(y(s_i) | y_{-i}, \mathcal{M}_g)$, but are derived using data excluding the k -th folder instead of just the i -th observation. The K -fold cross-validation Bayes predictor for $y(s_i)$ under model \mathcal{M}_g is $\hat{y}_g(s_i) = \mathbb{E}_g(y(s_i) | y[-k], \mathcal{M}_g) = h_g[-k]^T \hat{\gamma}_g[-k]$. For stacking of predictive densities, the optimal distribution changes into $\sum_{g=1}^G w_g p(y(s_i) | y[-k], \mathcal{M}_g)$.

3. THEORETICAL RESULTS

We focus on posterior inference for a Matérn model without trend to justify the stacking algorithms for these models. Subsequently, we extend these investigations to (2.2).

3.1. Posterior inference for the Matérn model. The Matérn model without trend is a special case of (2.1) with $\beta = 0$. Hence,

$$y(s) = z(s) + \varepsilon(s), \quad (3.1)$$

where $z(s)$ is modeled with the isotropic Matérn correlation function,

$$R_\Phi(s, s') := \frac{(\phi|s - s'|)^\nu}{\Gamma(\nu)2^{\nu-1}} K_\nu(\phi|s - s'|), \quad \Phi = \{\phi, \nu\}. \quad (3.2)$$

Here ϕ is the decay parameter, $\nu > 0$ is a fixed smoothness parameter, $\Gamma(\cdot)$ is the Gamma function, and $K_\nu(\cdot)$ is the modified Bessel function of the second kind of order ν (Abramowitz and Stegun, 1965, Section 10). We refer to (3.1) as the Matérn model with parameters $\{\sigma^2, \phi, \tau^2\}$. The conjugate Bayesian model (2.2) simplifies to

$$y | \sigma^2, \phi, \delta^2 \sim \mathcal{N}(0, \sigma^2(R_\phi(\chi) + \delta^2 I_n)), \quad \sigma^2 \sim \text{IG}(a_\sigma, b_\sigma). \quad (3.3)$$

We consider posterior inference for the conjugate Bayesian model (3.3) using (3.2). The following theorem shows the posterior inconsistency of the scale σ^2 under this model.

Theorem 3.1 (Posterior inference for the Matérn model). *Assume that the location set $\chi = \{s_1, \dots, s_n\}$ satisfies*

$$\max_{s \in \mathcal{D}} \min_{1 \leq i \leq n} |s - s_i| \asymp n^{-\frac{1}{d}}. \quad (3.4)$$

Let \mathbb{P}_0 be the probability distribution of the Matérn model (3.1) with $(\sigma_0^2, \phi_0, \tau_0^2)$. Under \mathbb{P}_0 ,

$$\lim_{n \rightarrow \infty} p(\sigma^2 | y(\chi), \phi, \delta^2) = \text{Dirac}(\tau_0^2 / \delta^2), \quad (3.5)$$

where $y(\chi) = (y(s_1), y(s_2), \dots, y(s_n))^T$, and $\text{Dirac}(\cdot)$ denotes the Dirac mass point. Consequently, $\lim_{n \rightarrow \infty} p(\tau^2 | y(\chi), \phi, \delta^2) = \text{Dirac}(\tau_0^2)$.

The asymptotic posterior inference of σ^2 is independent of the range decay ϕ chosen in the Matérn model. The scale σ^2 is posterior inconsistent unless the noise-to-spatial variance ratio $\delta^2 = \tau_0^2 / \sigma_0^2$, whereas the nugget τ^2 is posterior consistent. The proof of this theorem breaks into several lemmas. Recall the definition of $b_\sigma^* = b_{\sigma,n}^*$ from Lemma 2.1. The lemma below provides a simple expression for $b_{\sigma,n}^*$, which is specific to the Matérn model.

Lemma 3.2. *We have $b_{\sigma,n}^* = b_\sigma + \frac{1}{2}y(\chi)^T(\delta^2 I_n + R_\phi(\chi))^{-1}y(\chi)$.*

Proof. See Section A in the Supplement. □

The next lemma studies the asymptotic behavior of $b_{\sigma,n}^*$ when the range decay $\phi = \phi_0$; that is ϕ is fixed at the true value.

Lemma 3.3. *Let $\phi = \phi_0$, and assume that $\max_{s \in \mathcal{D}} \min_{1 \leq i \leq n} |s - s_i| \asymp n^{-\frac{1}{d}}$. Then*

$$\frac{b_{\sigma,n}^* - b_\sigma}{n} \longrightarrow \frac{\tau_0^2}{2\delta^2}, \quad \mathbb{P}_0\text{-almost surely.} \quad (3.6)$$

Proof. See Section A in the Supplement. □

Proof of Theorem 3.1. See Section A in the Supplement. □

3.2. Posterior prediction for the Matérn model. We consider Bayesian posterior predictive inference at a new location $s_0 \in \mathcal{D}$, under the Matérn model (3.2)–(3.3). We study the posterior predictive consistency of the conjugate model with the misspecified prefixed parameters. Let $Z_n(s_0)$ be a random variable distributed as $p(z(s_0) | y(\chi), \phi, \delta^2)$ and $Y_n(s_0)$ be distributed as $p(y(s_0) | y(\chi), \phi, \delta^2)$. We quantify the prediction error $\mathbb{E}_0(Z_n(s_0) - z(s_0))^2$ for the latent process and $\mathbb{E}_0(Y_n(s_0) - y(s_0))^2$ for the outcome variable, where $\mathbb{E}_0(\cdot)$ denotes expectation with respect to the Matérn model \mathbb{P}_0 .

Theorem 3.4 (Posterior predictive consistency for the Matérn model). *Let $s_0 \in \mathcal{D}$. For any given $\phi > 0$, denote $\text{Cov}(z, z(s_0) | \sigma^2)$ and $R_\phi(\chi)$ by $\sigma^2 J_{\phi,n}$ and $R_{\phi,n}$, respectively. Then,*

$$\mathbb{E}_0(Z_n(s_0) - z(s_0))^2 = E_{1,n} + E_{2,n} + o(1), \quad (3.7)$$

where $E_{1,n}$ is the prediction error of the best linear predictor for a Matérn model with any parameters $\{\sigma'^2, \phi, \tau'^2\}$ satisfying $\delta^2 = \frac{\tau'^2}{\sigma'^2}$, and

$$E_{2,n} := \frac{\tau_0^2}{\delta^2} [1 - J_{\phi,n}^T (\delta^2 I_n + R_{\phi,n})^{-1} J_{\phi,n}] \quad (3.8)$$

Consequently, if $E_{1,n}, E_{2,n} \rightarrow 0$ as $n \rightarrow \infty$, then the latent process $z(s)$ is posterior predictive consistent in the sense that $\mathbb{E}_0(Z_n(s_0) - z(s_0))^2 \rightarrow 0$ as $n \rightarrow \infty$ and, hence, $\mathbb{E}_0(Y_n(s_0) - y(s_0))^2 \rightarrow 2\tau_0^2$ as $n \rightarrow \infty$.

Proof. See Section B in the Supplement. □

Theorem 3.4 is similar in spirit to Zimmerman and Cressie (1992); Abt (1999), exploiting the rich structure of the Matérn model. In the decomposition (3.7), the term $E_{1,n}$ arises in the deviation from the posterior mean, whereas the term $E_{2,n}$ is from the posterior uncertainty. Moreover, the posterior mean of the Matérn model is identified as the best linear predictor of any Matérn model with parameters $\{\sigma'^2, \phi, \tau'^2\}$ provided $\tau'^2/\sigma'^2 = \delta^2$. This observation connects the Bayesian modeling to a frequentist approach in that the deviation error $E_{1,n}$ is viewed as the prediction error of the best linear predictor of a Matérn model in the presence of a nugget. However, the conditions $E_{1,n}, E_{2,n} \rightarrow 0$ are analytically intractable. Next we provide evidence to support these conditions which justify the posterior predictive consistency for the latent process.

The deviation error $E_{1,n}$: It is expected that the prediction error of the best linear predictor of a Matérn model in the presence of a nugget tends to 0 as long as the fill distance condition (3.4) holds. However, it is hard to prove this statement. To provide some ideas, we consider a one-dimensional example. We assume without loss of generality that $\mathcal{D} = [-1, 1]$, and $\chi = \{i/n, -n \leq i \leq n\}$ so the fill distance condition (3.4) is satisfied. Also let $\chi_\infty = \{i/n, -\infty < i < \infty\}$ be the infinite evenly spaced grid. Define

$$\hat{z} := \mathbb{E}(z(0) | y(s), s \in \chi \setminus \{0\}, \phi, \delta^2) \quad (\text{resp. } \hat{z}_\infty := \mathbb{E}(z(0) | y(s), s \in \chi_\infty \setminus \{0\}, \phi, \delta^2)),$$

be the best linear predictor of $z(0)$ based on the observations $y(s)$ on $\chi \setminus \{0\}$ (resp. $\chi_\infty \setminus \{0\}$). Note that \hat{z} (resp. \hat{z}_∞) can be computed using misspecified parameter values $\{\phi, \delta^2\}$. Let

$$e := \mathbb{E}_0(z(0) - \hat{z})^2 \quad (\text{resp. } e_\infty := \mathbb{E}_0(z(0) - \hat{z}_\infty)^2), \tag{3.9}$$

be the prediction error of the best linear predictor based on the observations on the finite grid $\chi \setminus \{0\}$ (resp. the infinite grid $\chi_\infty \setminus \{0\}$). We make the following assumption which relates e to e_∞ as $n \rightarrow \infty$.

Assumption 3.5 (Infinite approximation). *The difference $e - e_\infty \rightarrow 0$ as $n \rightarrow \infty$.*

This assumption suggests that as the grid becomes finer and finer, observations outside any fixed bounded interval have little impact on the prediction of $z(0)$. However, it is not easy to prove such a statement which is conjectured in (Stein, 1999, page 97). The plan is to prove $e_\infty \rightarrow 0$, and by Assumption 3.5 it implies that $e \rightarrow 0$ as $n \rightarrow \infty$. We formalize using the following proposition.

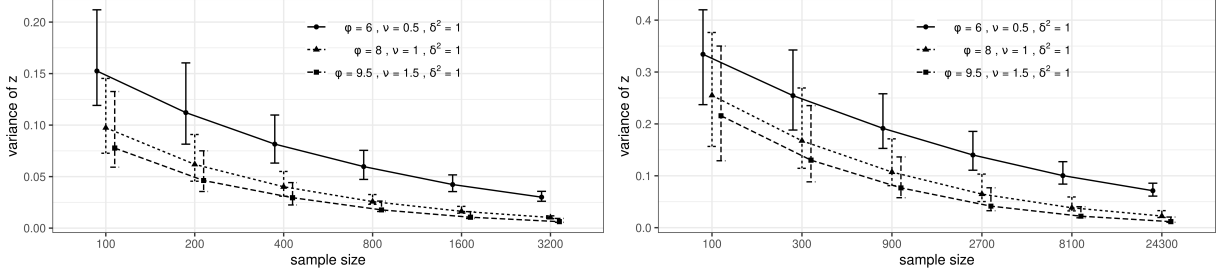


FIGURE 1. The median of $E_{2,n}$ for locations uniformly sampled on $[0, 1]$ (left) and $[0, 1]^2$ (right). The error bars indicate the 97.5th and 2.5th percentiles. The sample size n ranges from 100 to 3,200 and from 100 to 24,300 for the experiments on $[0, 1]$ and $[0, 1]^2$, respectively.

Proposition 3.6 (Prediction error for the Matérn model). *Let $\mathcal{D} = [-1, 1]$ and $\chi = \{i/n, -n \leq i \leq n\}$. Under Assumption 3.5, we have $e \rightarrow 0$ as $n \rightarrow \infty$, where e is the prediction error of the best linear predictor defined as in (3.9).*

Proof. See Section C in the Supplement. □

The posterior variance $E_{2,n}$: The error term $E_{2,n}$ defined by (3.8) is also analytically intractable. Here, we provide a numerical study to investigate the behavior of $E_{2,n}$ when $n \rightarrow \infty$ in the general case. We first generate the location set χ by uniformly sampling n locations in $[0, 1]$ or $[0, 1]^2$, then we compute $E_{2,n}$ for every location in χ with $\delta^2 = 1, \tau^2 = 1$ and different values of ϕ and ν . We expand the location set χ sequentially to sets with larger sample sizes by adding locations that are uniformly sampled in the study domain. For each expanded set χ , we recompute the $E_{2,n}$ for all locations in χ . Figure 1 plots the median, the 2.5th and 97.5th percentiles of $E_{2,n}$ for different sample sizes. The values of $E_{2,n}$ for points in a fixed domain, shown in Figure 1, decrease rapidly as the sample size increases, although the rate diminishes when d increases from 1 to 2. This suggests that the decreasing rate is related to the dimension.

3.3. Stacking algorithms. We attend to predictive inference using stacking. For ease of presentation, we focus on the LOO cross validation. Extending to K -fold cross validation is straightforward, albeit tedious. We offer the following result concerning the stacked mean square posterior prediction error.

Proposition 3.7 (Posterior prediction error for stacking). *Let $s_0 \in \mathcal{D}$, and $w^* := (w_1^*, \dots, w_G^*)$ be the stacking weights (e.g. defined by (2.6)) such that w_g^* is non-negative and $\sum_{g=1}^G w_g^* = 1$.*

Let the assumptions in Theorem 3.4 hold for each model \mathcal{M}_g . We have

$$\mathbb{E}_0 \left(y(s_0) - \sum_{g=1}^G w_g^* \mathbb{E}_g(y(s_0) | y) \right)^2 \rightarrow \tau_0^2 \quad \text{as } n \rightarrow \infty. \quad (3.10)$$

Proof. See Section D in the Supplement. □

The proof of Proposition 3.7 uses the posterior predictive consistency of $z(\cdot)$ (Theorem 3.4). It implies that if each candidate model yields reasonable prediction, then the stacking of means will also produce good predictive inference. Next, we show that the stacking predictor asymptotically minimizes the mean square posterior prediction error.

Theorem 3.8. *Let $s_0 \in \mathcal{D}$, and $w^* := (w_1^*, \dots, w_G^*)$ be the stacking weights (e.g. defined by (2.6)) such that w_g^* is non-negative and $\sum_{g=1}^G w_g^* = 1$. Let $E_{1,g,i} := \mathbb{E}_0(z(s_i) - \hat{y}_g(s_i))^2$, for $1 \leq g \leq G$ and $1 \leq i \leq n$ be the deviation error for the latent process $z(s)$ by leaving the i^{th} observation out under the model \mathcal{M}_g . Assume that for each $1 \leq g \leq G$*

$$\frac{1}{n} \sum_{i=1}^n E_{1,g,i} \rightarrow 0 \quad \text{as } n \rightarrow \infty. \quad (3.11)$$

Also, if the assumptions in Theorem 3.4 hold for each model \mathcal{M}_g , then as $n \rightarrow \infty$ we have

$$\mathbb{E}_0 \left(y(s_0) - \sum_{g=1}^G w_g^* \mathbb{E}_g(y(s_0) | y) \right)^2 - \mathbb{E}_0 \left(\frac{1}{n} \sum_{i=1}^n \left(y(s_i) - \sum_{g=1}^G w_g^* \hat{y}_g(s_i) \right)^2 \right) \rightarrow 0. \quad (3.12)$$

Proof. See Section E in the Supplement. □

Equation (3.11) implies that for each \mathcal{M}_g the average deviation error for the latent process goes to 0 as the sampling resolution becomes finer. This condition is consistent with the fact that in the one-dimensional grid we typically have $E_{1,g,i} \asymp \Delta^{\min(2\nu_0, \frac{2\nu}{2\nu+1})}$ (see Proposition 3.6); hence $\frac{1}{n} \sum_{i=1}^n E_{1,g,i} \rightarrow 0$ as $n \rightarrow \infty$. Theorem 3.8 holds for the candidate models with a misspecified smoothness parameter ν in the Matérn kernel for $d = 1$. Clyde and Iversen (2013) proves a similar result, while the established theoretical results about stacking assume exchangeability which is generally not available in geostatistical models. Lack of exchangeability limits formal theoretical developments. Section H offers limited discussion on stacking of predictive densities without exchangeable assumptions. Therefore, our theoretical results emerge from studying the behavior of the posterior and predictive distributions in the conjugate Bayesian linear model framework within the infill-paradigm. In this regard, our investigations differ from de Jonge and van Zanten (2013) who assume a true underlying function of arbitrary smoothness. The proof of Theorem 3.8 can be extended, fairly straightforwardly to the case where the LOO Bayes prediction $\hat{y}_g(s_i)$ is replaced by a much cheaper prediction based on K -fold cross-validation.

3.4. Stacked predictive densities in the general setting. We extend the discussion to the general conjugate Bayesian spatial model (2.2) and establish asymptotic results of the posterior distribution obtained through stacking. For easier exposition, we refine the notation for (2.3) by casting the spatial model in (2.2) into an augmented linear system. Let L_β be the Cholesky decomposition of V_β such that $V_\beta = L_\beta L_\beta^\top$, and L_Φ a non-singular square matrix such that $R_\Phi^{-1}(\chi) = L_\Phi^\top L_\Phi$. We adapt (2.2) as

$$\underbrace{\begin{bmatrix} \frac{1}{\delta} y \\ L_\beta^{-1} \mu_\beta \\ 0 \end{bmatrix}}_{y_\dagger} = \underbrace{\begin{bmatrix} \frac{1}{\delta} X & \frac{1}{\delta} I_n \\ L_\beta^{-1} & 0 \\ 0 & L_\Phi \end{bmatrix}}_{X_\dagger} \underbrace{\begin{bmatrix} \beta \\ z \end{bmatrix}}_{\gamma} + \underbrace{\begin{bmatrix} \eta_{\dagger,1} \\ \eta_{\dagger,2} \\ \eta_{\dagger,3} \end{bmatrix}}_{\eta_\dagger}, \quad (3.13)$$

where $\eta_\dagger \sim \mathcal{N}(0, \sigma^2 I_{2n+p})$ and $\sigma^2 \sim \text{IG}(a_\sigma, b_\sigma)$. This formulation simplifies the V_* matrix to an identity matrix. The conclusions detailed in Section 2.1 are applicable with the replacement of X_* and y_* by X_\dagger and y_\dagger . We use the equivalence of probability measures to explore posterior concentrations within an in-fill paradigm.

Assumption 3.9 (Equivalence). *Let \mathbb{P}_0 be the probability distribution of the process $y(s)$ defined by the model (2.1) with true parameter values $\{\beta_0, \sigma_0^2, \Phi_0, \tau_0^2\}$. For each Φ , there is $\sigma'^2 > 0$ such that the probability distribution of the process $y(s)$ defined by the model (2.1) with parameter values $\{\beta_0, \sigma'^2, \Phi, \tau_0^2\}$ is equivalent to \mathbb{P}_0 .*

The above Assumption holds when the latent process $z(s)$ follows a Matérn model in dimension $d \in \{1, 2, 3\}$. In this case, the probability distribution of the process $y(s)$ defined by the model (2.1) with parameters $\left\{ \beta_0, \frac{\sigma_0^2 \phi_0^{2\nu}}{\phi^{2\nu}}, \phi, \tau_0^2 \right\}$ is equivalent to \mathbb{P}_0 (see e.g. Tang et al. (2021, Section 2.1)). We denote $\mathbb{E}_0(\cdot)$ the expectation with respect to \mathbb{P}_0 .

Posterior inference: The following theorem, which extends Theorem 3.1, explores the posterior (in)consistency of the scale σ^2 .

Theorem 3.10 (Posterior inference (in)consistency). *Let \mathbb{P}_0 be the probability measure of the model (2.1) with parameter values $\{\beta_0, \sigma_0^2, \Phi_0, \tau_0^2\}$, and let Assumption 3.9 hold. Let $H = X_\dagger (X_\dagger^\top X_\dagger)^{-1} X_\dagger^\top$ be the $(2n+p) \times (2n+p)$ orthogonal projector onto the column space of X_\dagger and let $H = \begin{bmatrix} H_{11} & H_{12} \\ H_{12}^\top & H_{22} \end{bmatrix}$ be a 2×2 partition of H so that H_{22} is the lower right $n \times n$ block formed by rows and columns indexed from $n+p+1$ to $2n+p$. Assume that $\text{Tr}(H_{22})/n \rightarrow \alpha$ as $n \rightarrow \infty$. Then under \mathbb{P}_0 ,*

$$\lim_{n \rightarrow \infty} p(\sigma^2 | y(\chi)) = \text{Dirac}(\sigma_\alpha^2), \quad (3.14)$$

where $\sigma_\alpha^2 := \frac{\tau_0^2}{\delta^2} \alpha + \sigma'^2 (1 - \alpha)$.

Proof. See Section F in the Supplement. □

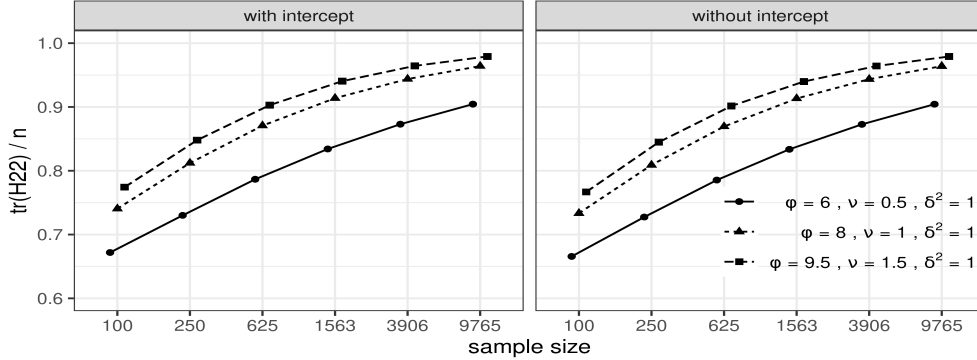


FIGURE 2. Plots of $\text{Tr}(H_{22})/n$ when $x(s)$ consists of an intercept only (left), and with additional covariates (right) for different parameter values.

Similar to the Matérn model, Theorem 3.10 suggests that the posterior distribution of the scale parameter σ^2 in the general conjugate model does not necessarily concentrate on the true generating value. The parameter α quantifies how the trend and the chosen parameter Φ affects the inference on σ^2 . Our analysis reveals that the posterior distribution for σ^2 approaches a value influenced by δ^2 as sample size increases. This is especially pronounced when the stacking weights for the candidate models exhibit variability in their respective δ^2 values, leading to an anticipation of multi-modality in the stacked posterior density of σ^2 . Such multi-modality suggests that employing a stacking algorithm may not yield dependable posterior inferences for σ^2 , underscoring limitations in stacking over fixed values of σ^2 .

The assumption $\text{Tr}(H_{22})/n \rightarrow \alpha$ is generally hard to check analytically. Figure 2 summarizes some numerical experiments to empirically explore these assumptions. The study domain \mathcal{D} is $[0, 1]^2$, and locations in χ are chosen uniformly on \mathcal{D} . We generate data using the Matérn covariogram for $z(s)$ (see (3.2) in Section 2.1). We consider two types of predictors $x(s)$. For the first type, titled “with intercept”, $x(s)$ consists of a constant 1 for intercept and a predictor generated by a standard normal. For the second type, labeled “without intercept”, $x(s)$ is composed of two predictors sampled from a standard normal. We consider the trends of the target quantities with different hyper-parameter values in the covariogram of $z(s)$ and different types of $x(s)$ as sample size increases. Figure 2 shows that $\text{Tr}(H_{22})/n$ increases as sample size increases for all examples. Since $\text{Tr}(H_{22})/n$ is bounded above by 1, the assumption $\text{Tr}(H_{22})/n \rightarrow \alpha$ for some constant α is likely to hold in general. This is consistent with Theorem 3.1, where σ^2 converges to the Dirac measure at τ_0^2/δ^2 .

Posterior prediction: We can extend Theorem 3.8 by establishing consistent posterior predictions using the general conjugate Bayesian spatial models. Supplement G offers further developments regarding the corresponding asymptotic results. However, verifying the conditions necessary for posterior predictive consistency is challenging, which diminishes their

practical relevance. Section 5 presents simulations showing that stacking algorithms serve as efficient alternatives to more expensive MCMC algorithms.

4. IMPLEMENTATION OF STACKING ALGORITHMS

We outline algorithms that compute the weights for spatial stacking. We first partition the data into K -folds based on locations. Let $X = [x(s_1) : \dots : x(s_n)]^T$ be the design matrix with $X[k]$, $y[k]$ and $\chi[k]$ denoting the predictors, outcome and observed locations from k -th fold, respectively, and $X[-k]$, $y[-k]$ and $\chi[-k]$ denoting respective data not in k -th fold. Let n_k be the number of observed locations for the k -th fold. The values of the prefixed hyper-parameters $\{\phi, \nu, \delta^2\}$ of the conjugate Bayesian spatial regression model are picked from the grid G_{all} , which is expanded over the grids of candidate values as the Cartesian product $G_\phi \times G_\nu \times G_\delta^2$ for $\{\phi, \nu, \delta^2\}$. We compute the posterior expectation $\mathbb{E}(y[k] | y[-k], \phi, \nu, \delta^2)$ for $k = 1, \dots, K$ and all candidate $\{\phi, \nu, \delta^2\}$ when using stacking of means to obtain the stacking weights. Algorithm 1 describes the procedure. Algorithm 1 structures the computation for different choices of δ^2 to be nested in each folder k . This structure allows the re-use of the correlation matrix for the same $\{\phi, \nu\}$ in the same folder for different δ^2 , but it only works for the shared candidate values G_δ^2 . Solving for the weights is a quadratic programming problem (Appendix L). We use the *solve.QP()* function offered by the *quadprog* package in the R statistical computing environment and the solver *Mosek* (Andersen and Andersen, 2000) to solve for the weights in R and Julia.

We obtain the stacking weights for predictive densities by evaluating the log point-wise predictive density, $(lp_{(\phi, \nu, \delta^2)}(s))$, of $y(s)$ for all locations in each fold for all candidate models. The log point-wise predictive density is derived explicitly in Appendix I, while Appendix J devises a Monte Carlo algorithm for stacking of predictive densities. The stacking weights for predictive densities are calculated using *Mosek* in R and Julia implementations. Algorithm 2 summarizes the procedure. Posterior inference for quantities of interest subsequently proceed from the “stacked posterior”,

$$\tilde{p}(\cdot | y) = \sum_{l=1}^L \hat{w}_l p(\cdot | y, \mathcal{M}_g), \quad (4.1)$$

where \hat{w}_l are the optimal weights obtained using Algorithm 1 or 2.

While inferential performance of these algorithms is promising (theoretically and asymptotically) when the candidate values of the correlation parameters fall in a reasonable domain, the choice of G_ϕ , G_ν and G_δ^2 still impact the performance of stacking in practical analysis. Here, we offer guidance on specifying $G_\phi, G_\nu, G_\delta^2$. More comprehensive evaluation and discussion are presented in Section 5. Based on the property of Matérn kernel, popular choices for ν include 0.5, 1.0, 1.5 and 1.75 or 2. Matérn kernels with $\nu > 2$ generate overly smoothed

Algorithm 1 Stacking weights calculation using stacking of means

- 1: **Input:** X, y, χ : Design matrix, outcome and location set $\mu_\beta, V_\beta, a_\sigma, b_\sigma$: Prior parameters; $G_\phi, G_\nu, G_{\delta^2}$: Grids of ϕ, ν, δ^2 ; K : Number of folders
 - 2: **Output:** $w = \{w_{\phi, \nu, \delta^2}\}_{(\phi, \nu, \delta^2) \in G_{all}}$: Stacking weights; G_{all} : Grid spanned by $G_\phi, G_\nu, G_{\delta^2}$
 - 3: **function** SPSTACKING($X, y, \chi, \mu_\beta, V_\beta, a_\sigma, b_\sigma, G_\phi, G_\nu, G_{\delta^2}, \phi, \nu, \delta^2, K$)
 - 4: Compute $X_{\text{prod}}^{(k)} = X^\top[-k]X[-k]$, $X_y^{(k)} = X^\top[-k]y[-k]$ and record the number of observations n_k in fold k for $k = 1, \dots, K$, where $X[-k]$ $y[-k]$ denotes the predictors and response for observations not in fold k
 - 5: **for** $\Phi = \{\phi, \nu\}$ in grid expanded by G_ϕ and G_ν **do**
 - 6: **for** $k = 1$ to K **do**
 - 7: Calculate $R_\Phi^{-1}(\chi[-k]) = (R_\Phi(s, s'))_{s, s' \in \chi[-k]}^{-1}$ $\mathcal{O}(n^3)$
 - 8: Store $J_\Phi(\chi[k], \chi[-k]) = (R_\Phi(s, s'))_{s \in \chi[k], s' \in \chi[-k]}$
 - 9: **for** δ^2 in $G_{\delta^2}^2$ **do**
 - 10: Compute the Cholesky factor L_* of
 - 11:
$$M_*^{-1} = L_* L_*^\top = \begin{bmatrix} \delta^{-2} X_{\text{prod}}^{(k)} + V_\beta^{-1} & \delta^{-2} X^\top[-k] \\ \delta^{-2} X[-k] & R_\Phi^{-1}(\chi[-k]) + \delta^{-2} I_{n-n_k} \end{bmatrix}$$
 $\mathcal{O}(n^3)$
 - 12: Compute $u = m_* = \begin{bmatrix} V_\beta^{-1} \mu_\beta + \delta^{-2} X_y^{(k)} \\ \delta^{-2} y[-k] \end{bmatrix}$
 - 13: Solve $L_*^* x = u$ by forward solver and solve $L_*^\top u = x$ using backward solver
 - 14: Set $\begin{bmatrix} \mu_\beta^* \\ \mu_z^* \end{bmatrix} \leftarrow \begin{bmatrix} u_1 \\ u_2 \end{bmatrix} = u$
 - 15: Compute expected outcome on locations in fold k
 - 16: $\mathbb{E}(y[k] | y[-k], \Phi, \delta^2) = X[k] \mu_\beta^* + J_\Phi(\chi[k], \chi[-k]) \cdot R_\Phi^{-1}(\chi[-k]) \cdot \mu_z^*$
 - 17: Compute stacking weights w based on $\{\mathbb{E}(y[k] | y[-k], \phi, \nu, \delta^2)\}_{(\phi, \nu, \delta^2) \in G_{all}}^{k=1, \dots, K}$ using quadratic programming (QP). Appendix L offers further details.
 - 18: **return** $\{w, G_{all}\}$,
-

processes and cause numerical instabilities. The range of candidate values for ϕ are determined by a lower and upper bound of range along with the choices for ν . In simulations, we choose equally spaced candidate values for G_ϕ . We note that an even grid is not equivalent to a uniform prior unlike, for example, Kazianka and Pilz (2012). G_ϕ serves as a discretized domain for ϕ and, as we described and showed in Appendix M.3, one can hardly obtain inference about hyper-parameters through stacking. The choice of candidate values for δ^2 is more subtle. In our implementation, we use quantiles of beta distribution $\text{Beta}(a_1, a_2)$ to select candidate values of $\delta^2/(1 + \delta^2)$, which falls between 0 and 1. This is based on the fact that when $\sigma^2 \sim \text{IG}(a_1, b)$, $\tau^2 \sim \text{IG}(a_2, b)$ and the two parameters are independent, $\delta^2/(1 + \delta^2) \sim \text{Beta}(a_1, a_2)$. The two shape parameters a_1, a_2 are determined from values of

Algorithm 2 Stacking weights calculation using stacking of predictive densities

- 1: **Input:** X, y, χ : Design matrix, outcome and location set; $\mu_\beta, V_\beta, a_\sigma, b_\sigma$: Prior parameters; $G_\phi, G_\nu, G_{\delta^2}$: Grids of ϕ, ν, δ^2 ; K : Number of folders
 - 2: **Output:** $w = \{w_{\phi, \nu, \delta^2}\}_{(\phi, \nu, \delta^2) \in G_{all}}$: Stacking weights; G_{all} : Grid spanned by $G_\phi, G_\nu, G_{\delta^2}$
 - 3: **function** SPSTACKING($X, y, \chi, \mu_\beta, V_\beta, a_\sigma, b_\sigma, G_\phi, G_\nu, G_{\delta^2}, \phi, \nu, \delta^2, K$)
 - 4: Compute $X_{\text{prod}}^{(k)} = X^\top[-k]X[-k]$, $X_y^{(k)} = X^\top[-k]y[-k]$, $\|y[-k]\|^2 = y^\top[-k]y[-k]$ and record the number of observations n_k in fold k for $k = 1, \dots, K$, where $X[-k]$ $y[-k]$ denotes the predictors and response for observations not in fold k
 - 5: **for** $\Phi = \{\phi, \nu\}$ in grid expanded by G_ϕ and G_ν **do**
 - 6: **for** $k = 1$ to K **do**
 - 7: Calculate $R_\Phi^{-1}(\chi[-k]) = (R_\Phi^{-1}(s, s'))_{s, s' \in \chi[-k]}$ $\mathcal{O}(n^3)$
 - 8: Store $J_\Phi(\chi[k], \chi[-k]) = (R_\Phi(s, s'))_{s \in \chi[k], s' \in \chi[-k]}$
 - 9: **for** δ^2 in G_δ^2 **do**
 - 10: Compute the Cholesky decomposition L_* of
 - 11:
$$M_*^{-1} = L_* L_*^\top = \begin{bmatrix} \delta^{-2} X_{\text{prod}}^{(k)} + V_\beta^{-1} & \delta^{-2} X^\top[-k] \\ \delta^{-2} X[-k] & R_\Phi^{-1}(\chi[-k]) + \delta^{-2} I_{n-n_k} \end{bmatrix}$$
 $\mathcal{O}(n^3)$
 - 12: Compute $x = m_* = \begin{bmatrix} V_\beta^{-1} \mu_\beta + \delta^{-2} X_y^{(k)} \\ \delta^{-2} y[-k] \end{bmatrix}$
 - 13: Solve $L_* u = x$ by forward solver
 - 14: Compute $b_* = b_\sigma + 0.5(\delta^{-2} \|y[-k]\|^2 + \mu_\beta^\top V_\beta^{-1} \mu_\beta - u^\top u)$ and
 - 15: $a_* = a_\sigma + 0.5(N - n_k)$
 - 16: Solve $L_*^\top x = u$ by backward solver; set $\begin{bmatrix} \mu_\beta^* \\ \mu_z^* \end{bmatrix} \leftarrow \begin{bmatrix} x_1 \\ x_2 \end{bmatrix} = x$
 - 17: Generate the posterior expected outcome on locations in fold k
 - 18: $\mathbb{E}(y[k] | y[-k], \Phi, \delta^2) = X[k] \cdot \mu_\beta^* + J_\Phi(\chi[k], \chi[-k]) \cdot R_\Phi^{-1}(\chi[-k]) \cdot \mu_z^*$
 - 19: Compute $lpc = -0.5 \log(2\pi) + \log \Gamma(a_* + 1/2) - \log \Gamma(a_*) + a_* \log b_*$
 - 20: **for** $s \in S[k]$ **do**
 - 21: Generate $h_s = \begin{bmatrix} x(s) & J_\Phi(s, \chi[-k]) \cdot R_\Phi^{-1}(\chi[-k]) \end{bmatrix}$ where $J_\Phi(s, \chi[-k])$
 - 22: is the row with elements $(R_\Phi(s, s'))_{s' \in \chi[-k]}$
 - 23: Compute $V_s = \|L_*^{-1} h_s^\top\|^2 + \delta^2$.
 - 24: Compute the log point-wise predictive density of $y(s)$ at location s ,
 - 25: by (I.1): $lp_{(\phi, \nu, \delta^2)}(s) = lpc - 0.5 \log(V_s) -$
 - 26: $(a_* + 1/2) \log\{b_* + (y(s) - \mathbb{E}(y(s) | y[-k], \phi, \nu, \delta^2))^2 / (2V_s)\}$
 - 27: Solve convex optimization problem: Under constrains $\sum_{(\phi, \nu, \delta^2) \in G_{all}} w_{(\phi, \nu, \delta^2)} = 1$ and $w_{(\phi, \nu, \delta^2)} > 0$, maximize $\sum_{s \in \chi} \log(\sum_{(\phi, \nu, \delta^2) \in G_{all}} \exp\{lp_{(\phi, \nu, \delta^2)}(s)\} * w_{(\phi, \nu, \delta^2)})$
 - 28: **return** $\{w, G_{all}\}$,
-

nugget and partial sill estimated from an empirical semivariogram. We choose b to be the larger value of the estimated nugget and partial sill in our implementation. Since the posteriors of σ^2 and τ^2 are not independent, other choices for G_δ^2 are preferred when additional information about δ^2 is available.

5. SIMULATION

5.1. Simulation settings. We present two simulation experiments to evaluate predictive performance using our stacking algorithms. The data for these experiments are generated using (2.1) on locations sampled uniformly over a unit square $[0, 1]^2$ with R_ϕ being the Matérn covariogram in (3.2). The sample size n of the simulated data sets ranges from 200 to 900, and we randomly pick $n_h = 100$ observations for checking predictive performance. The vector $x(s)$ consists of an intercept and a predictor generated from a standard normal distribution. We use the parameter values $\beta = (1, 2)^\top$, $\phi = 7$, $\sigma^2 = 1$, $\tau^2 = 1$ and $\nu = 1$ to generate data for the first simulation, and $\phi = 20$, $\sigma^2 = 1$, $\tau^2 = 0.3$ and $\nu = 0.5$ for the second.

We analyze our data using the $K = 10$ -fold stacking Algorithms 1 and 2 with candidate values $\nu \in G_\nu = \{0.5, 1, 1.5, 1.75\}$. The candidate values for ϕ are selected so that the “effective spatial range”, which refers to the distance where spatial correlation drops below 0.05, covers 0.1 and 0.6 times $\sqrt{2}$ (the maximum inter-site distance within a unit square) for all candidate values of ν . Here we set $G_\phi = \{3, 14, 25, 36\}$. Finally, we specify G_{δ^2} to comprise the 0.05, 0.35, 0.65 and 0.95th quantiles of a beta distribution with expectations of σ^2 and τ^2 equal to their data generating values. We assign an $\text{IG}(a_\sigma, b_\sigma)$ prior with $a_\sigma = b_\sigma = 2$ for σ^2 . The prior of β is $\text{N}(\mu_\beta, V_\beta)$ where $\mu_\beta = 0$ and $V_\beta = 4 \cdot I$. For each simulated data set, we implement stacking of means and of predictive densities to obtain the expected outcome $\hat{y}(s)$ based on the held out observed locations. The predictive accuracy is evaluated by the root mean squared prediction error over a set of n_h hold-out locations in set \mathcal{S}_h ($\text{RMSPE} = \sqrt{\sum_{s \in \mathcal{S}_h} ((\hat{y}(s) - y(s))^2) / n_h}$). We also compute the posterior expected values of the latent process $\hat{z}(s)$ for $z(s)$ on all of the n sampled locations in \mathcal{S} and evaluate the root mean squared error for $z(s)$ ($\text{RMSEZ} = \sqrt{\sum_{s \in \mathcal{S}} (\hat{z}(s) - z(s))^2 / n}$). To further evaluate the distribution of predicted values, we compute the mean log point-wise predictive density for the n_h held out locations ($\text{MLPD} = \sum_{s \in \mathcal{S}_h} \{\log(\sum_{g=1}^G w_g p(y(s) | y, \mathcal{M}_g))\} / n_h$).

Apart from stacking, we also implement a fully Bayesian model with priors on the hyperparameters using Markov chain Monte Carlo (MCMC) sampling for comparison. In addition, we carry out exact Bayesian inference using the conjugate model in Section 2.1 with hyperparameters fixed at the exact value (denoted as \mathcal{M}_0). We use the same priors for σ^2 and β as those in stacking implementations. For the rest of the priors needed in full MCMC sampling, we assign uniform priors $\text{U}(3, 36)$ for ϕ and $\text{U}(0.25, 2)$ for ν , and an $\text{IG}(2, 2)$ prior for τ^2 . Sampling is fitted through the *spLM* function in the *spBayes* package in R. The diagnostic metrics are computed based on 1,000 posterior samples retained after convergence was diagnosed over a burn-in period of 10,000 initial iterations. The algorithm for recovering the expected z and the log point-wise predictive density based on the output of *spLM* is presented in Appendix K of the Supplement. We monitor all diagnostic metrics for prediction for all

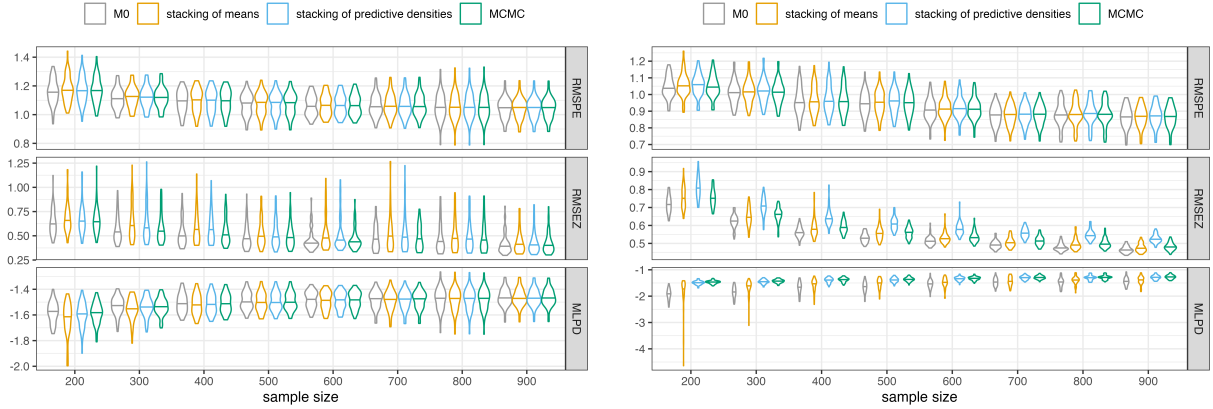


FIGURE 3. *Distributions of the diagnostic metrics for prediction performance for the first simulation (left) and the second simulation (right). Each distribution is depicted through a violin plot. The horizontal line in each violin plot indicates the median.*

competing algorithms. To measure uncertainty of the diagnostic metrics, we generate 60 data sets for each sample size in each simulation, fit each data set with the four competing methods and record the diagnostic metrics of each model fitting.

5.2. Predictive performances. The aforementioned methods exhibit different behaviors in the two simulation studies. Figure 3 compares predictive performance. There are no pronounced distinctions in predictive performance among the competing models in the first simulation. In the second simulation, however, stacking of means seems to deliver better estimates for the latent process at observed and unobserved locations than stacking of predictive densities (based on RMSEZ), while stacking of predictive densities outperforms stacking of means in terms of the log point-wise predictive density (based on MLPD). This is unsurprising as we optimize prediction error in the stacking of means and we maximize the log predictive densities in the stacking of predictive densities. Treating the fully Bayesian model with priors on all hyperparameters (fitted using MCMC) as a benchmark, we find that stacking of predictive densities is very competitive in terms of MLPD. The performance of latent process estimation for the full Bayesian model falls between stacking of means and stacking of predictive densities. All competing algorithms deliver very similar prediction accuracy for the outcome at unobserved locations, while stacking of means slightly outperforms the full Bayesian model with regard to the medians of the RMSPEs for all fittings; both are slightly better than stacking of predictive densities, The conjugate Bayesian model M_0 provides the best point estimates for the outcome and latent processes based on RMSPE and RMSEZ, but is less impressive in terms of MLPD. These results indicate that stacking of means is

excels in point estimation, while stacking of predictive densities is preferable for interval estimation.

We check the counts of the non-zero weights in stacking and find that stacking of means tends to produce a slightly smaller number of non-zero weights than stacking of predictive densities. The number of non-zero weights is small for both stacking algorithms and this phenomenon is also observed and discussed in Breiman (1996). On average, there are around 3.6 and 4.3 out of 64 weights that are greater than 0.001 in the simulation studies for stacking of means and stacking of predictive densities, respectively. This number is relatively consistent when the sample sizes increase. Plots for the distributions of nonzero weights counts are provided in Figure 10. These results suggest that stacking methodology is memory efficient, which is beneficial for large-scale spatial data analysis.

Building on the preceding broader analysis, we now attend to more specific scrutiny of inferential performance. We examine a case from Simulation 1 featuring 800 observations and another from Simulation 2 with 400 observations to enhance our evaluation of stacking’s predictive performance. Figure 4 directly compares 95% credible intervals (CIs) and point estimates obtained through stacking and MCMC methods. Stacking of predictive density appears to closely align with inference from MCMC, while stacking of means tends to marginally underestimate the CI widths, particularly in the setting with smaller sample size.

Appendix M.2 illustrates the interpolated maps of the predicted outcome at held out locations and the expected latent processes over all locations generated by different fitting algorithms. The posterior predictive means, $\mathbb{E}(y(s) | y)$, and $\mathbb{E}(z(s) | y)$, share similar patterns with the raw data. The mean of $z(s)$ estimated by stacking of predictive densities appears smoother than those estimated from \mathcal{M}_0 , full Bayes and stacking of means, while the predicted mean of $y(s)$ at unobserved locations are indistinguishable across all methods.

5.3. Running time comparisons. Computer programs for reproducing the simulation studies are hosted in the GitHub repository https://github.com/LuZhangstat/spatial_stacking. Comparisons in predictive performances presented above are conducted in R. For the running time comparisons reported here, the stacking algorithms are implemented using `Julia-1.6.6` and the MCMC sampling algorithms are executed in `R-4.2.0`. We report the time for obtaining weights for stacking, and we consider the sampling time for $\{\phi, \nu, \sigma^2, \tau^2\}$ using MCMC (no sampling of $\{\beta, z\}$ and no predictions). The timing comparisons are based upon experiments on a Windows 10 pro platform, with 64 GB of RAM and a 1-Intel Core i7-7700K CPU @ 4.20GHz processor with 4 cores each and 2 threads per core—totaling 8 possible threads for parallel computing. Figure 5 summarizes the running time for the three competing algorithms. On average, the stacking of means is 526 times faster than MCMC, while stacking of predictive densities is only slightly slower being around 430 times faster than MCMC sampling. These experiments clearly establish that predictive stacking

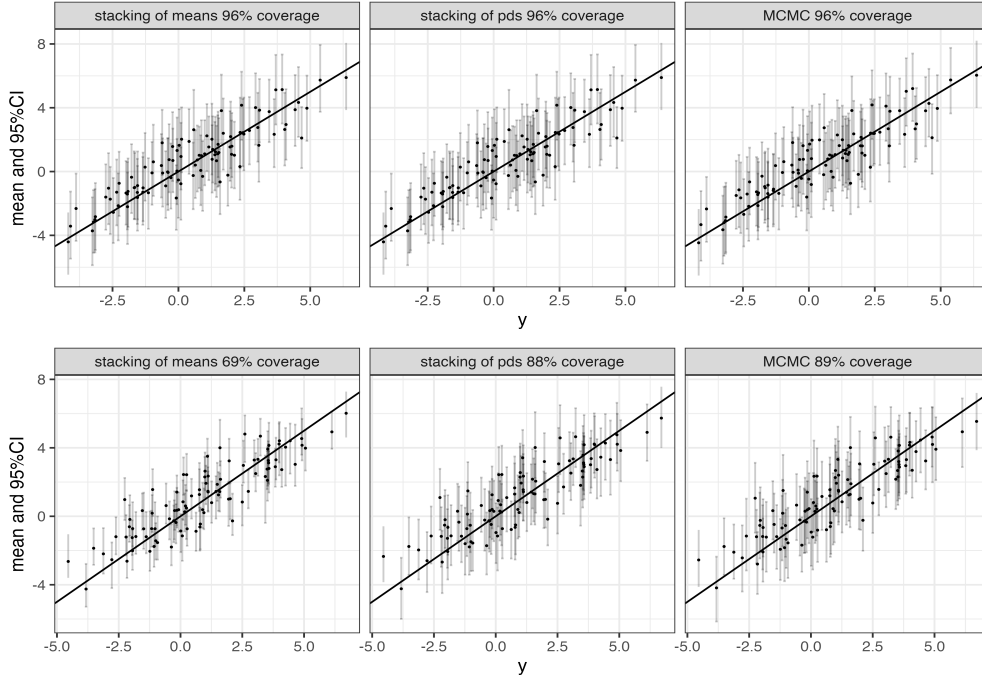


FIGURE 4. Scatterplots for predicted versus actual outcomes at 100 unobserved locations with 95% credible intervals from Simulation 1 with 800 observations (upper row) and another example from Simulation 2 with 400 observations (lower row). Each plot includes a solid black line representing the 45-degree reference line, with titles indicating 95% CI coverage. 'pds' denotes predictive densities.

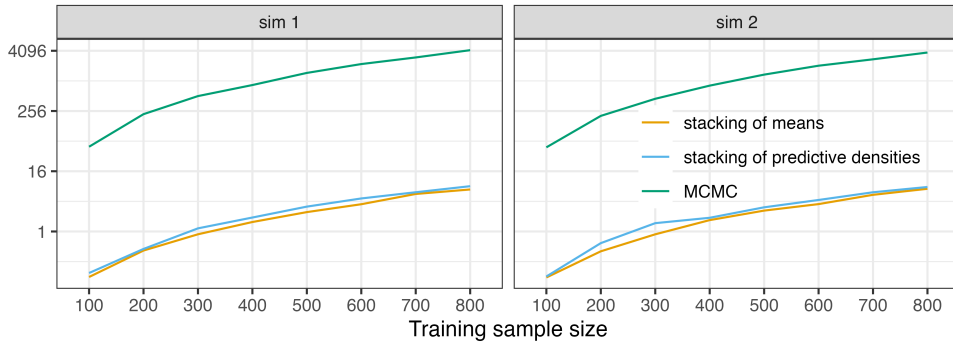


FIGURE 5. Running time comparison for stacking and MCMC sampling

algorithms are efficient alternatives to MCMC for estimating latent spatial processes and predicting spatial outcomes.

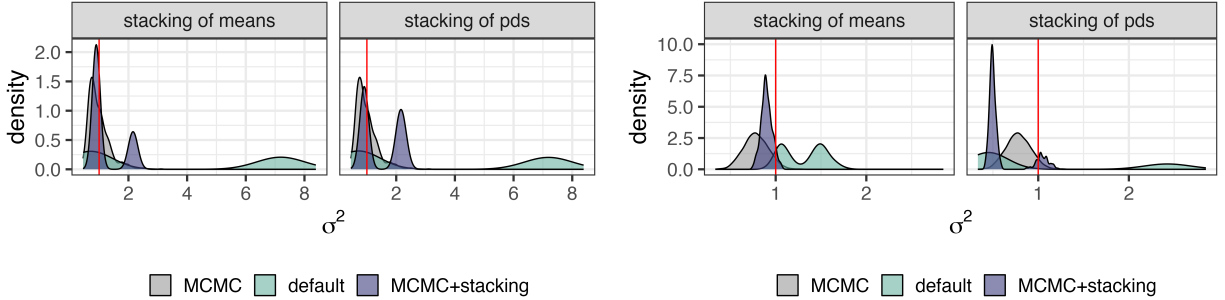


FIGURE 6. Densities of σ^2 for the example with 800 observations from simulation 1 (left) and the example with 400 observations from simulation 2 (right). Vertical red lines indicate the actual σ^2 values. Grey densities represent MCMC-recovered posterior distributions of σ^2 . ‘Default’ and ‘MCMC+Stacking’ show stacking results using two methods for selecting ϕ, ν, δ^2 candidates. Left panel: stacking of means. Right panel: stacking of predictive densities.

We further explore improving inferential performance of stacking by judicious choices of $\{\phi, \nu, \delta^2\}$. We explore the inferential impact of selecting candidate values for the prefixed hyperparameters from their posterior distributions. These posterior distributions are evaluated from MCMC samples of the full Bayesian model. The method for choosing candidate values as outlined in previous subsections is now referred to as the ‘default’ method. Given that the default algorithm in the simulation studies involves 64 candidate models, we randomly select 64 samples of $\{\phi, \nu, \delta^2\}$ as candidate values. Although obtaining marginal posterior samples is impractical when implementing the stacking algorithm, this approach serves as our benchmark, assuming full knowledge of the marginal posterior. We also present the posterior distributions recovered by MCMC as the gold standard for comparisons.

Figure 18 depicts a comparison of diagnostic metrics and reveals that there is no significant improvement in predictive performance by selecting the prefixed correlation parameters through posterior distributions. To further check the impact, we revisit the two selected examples in Section 5.2, featuring 800 and 400 observations from simulations 1 and 2, respectively. Figure 6 compares the posterior distributions for σ^2 . Regardless of the method used for selecting candidate values for the prefixed hyper-parameters, the marginal distributions recovered through stacking invariably exhibits multimodal behavior. This reinforces the claim that stacking does not provide effective inference for covariance parameters, including σ^2 . Furthermore, we observe that the distribution of σ^2 recovered by stacking is highly dependent on the choice of candidate values for the correlation parameter. Similarly, for τ^2 , we observe multimodality in the case with a smaller sample size, as shown in Figure 19. Intriguingly, the variations in the distribution of σ^2 resulting from stacking do not impact the

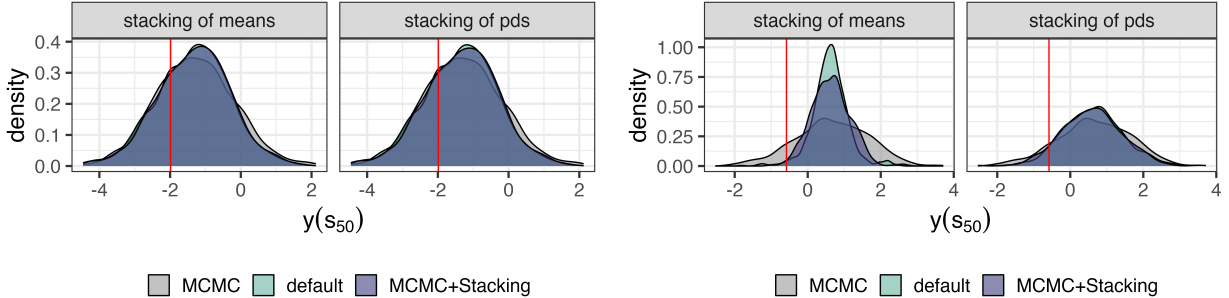


FIGURE 7. *Predictive densities of the outcome at 50-th point in the example with 800 observations from simulation 1 (left) and the example with 400 observations from simulation 2 (right). Vertical red lines indicate the actual values. Grey densities represent MCMC-recovered posterior distributions. 'Default' and 'MCMC+Stacking' show stacking results using two methods for selecting ϕ, ν, δ^2 candidates. Left panel: stacking of means. Right panel: stacking of predictive densities*

predictive distribution of outcomes. We examine the predictive distribution of the outcome at several unobserved points and present some typical examples in Figure 7. The predictive distributions obtained from stacking are largely consistent regardless of hyperparameter selection methods. Additionally, the predictive distributions recovered by stacking of means tend to concentrate around the mode compared to those recovered by stacking of predictive densities. The distributions for the intercept recovered by stacking may have larger variance according to Figure 20, while those for regression coefficients β_2 closely align with inference from MCMC. We conclude that the improvement of selecting candidate values for $\{\phi, \delta^2, \nu\}$ from the posterior is limited based on these results.

6. AOD PREDICTION

We use $K = 10$ -fold Bayesian stacking to analyze Aerosol Optical Depth (AOD) observations from satellite technologies in global aerosol research. This is an increasingly important field across multiple disciplines such as environmental health, climatology, atmospheric science, and remote sensing (Voiland, 2010). Unlike ground-based monitoring that is limited by regional coverage and budget, satellite-derived AOD data provides a more expansive picture of aerosol distributions on a global scale. However, cloud screening and conditions of high surface reflectance can result in a significant proportion of missing data in AOD satellite observations (Li et al., 2009). Prevailing AOD interpolation algorithms often rely upon random forests and neural networks (Fan and Sun, 2023; Aguilera et al., 2023). Nonetheless, Gaussian process models present a competitive alternative by accommodating data-driven

processes and providing essential uncertainty quantification. We apply our Bayesian spatial regression model using stacking to analyze 1-km MODIS AOD products (MCD19A2) over the Greater Los Angeles area (Lyapustin et al., 2018) and assess their predictive performances in the context of large-scale AOD retrieval and uncertainty quantification.

Figure 8 is a base image with near-complete AOD coverage on September, 13th, 2018, encompassing 16,003 pixels that do not encroach over water bodies. We use the cloud pattern from August, 24th, 2018, to partition the data. Pixels not obscured by clouds comprise the training set (totaling 11,857 pixels), while the remaining 4,146 pixels form the testing set. We use log-transformed AOD as the outcome and five predictors (resampled to a 1-km resolution): the x-y coordinates, the Enhanced Vegetation Index (EVI) from the 16-day MODIS MOD13A2 products, the impervious surface percentage from the USGS National Land Cover Database (NLCD) 2018, and the weighted road network density from OpenStreetMap (Figure 8).

Following the prototype in simulation studies, we set $G_\nu = (0.5, 1.0, 1.5, 1.75)$. The candidate values for ϕ were set at $(0.1, 0.4, 0.7, 1.0)$ so that the practical range of the process spans from 5km to 25km. This range was conservatively estimated based on the empirical semivariogram of the residual of a linear regression model (Figure 21). We used the estimated values for σ^2 and τ^2 from the empirical semivariogram to determine G_{δ^2} . We assigned $\sigma^2 \sim \text{IG}(2, 0.05)$ and the remaining settings following those used in our simulation studies. In addition to stacking, we expanded the analysis by including five competitive algorithms: Deep Learning, Random Forest (RF) (Breiman, 2001), Gradient Boosting Machine (GBM) (Friedman, 2001), an Ensemble Model integrating the aforementioned three algorithms, and Bayesian Linear Regression (BLR) without spatial effects. We implemented the first four algorithms on H2O (Cook, 2016), a popular open-source platform designed for big data analytics. Specifically, we utilized H2O’s default settings for the Deep Learning algorithm (Candel et al., 2016) and similarly for the GBM. For the RF model, we determined the optimal configuration, setting the number of trees to 120 and the maximum tree depth to 60—via a Cartesian grid search. We validated these learner models with 10-fold cross-validation. H2O’s Ensemble method is another stacking algorithm which finds the optimal combination of predictions from the fitted DL, RF and GBM models. The BLR model was fitted through R package `brms`. We assigned $N(0, 2^2)$ to our regression coefficients and a half-Cauchy prior half-Cauchy(0, 0.5) to the standard deviation of the error.

For stacking and BLR, the AOD interpolation was retrieved using posterior mean. We calculated the root mean squared prediction error (RMSPE), mean absolute error (MAE) and Pearson correlation coefficient (R) by comparing the interpolated AOD with the testing data AOD, and we have summarized these results in Table 1. The two stacking algorithms significantly outperformed the other competitive algorithms in terms of Pearson correlation coefficients, RMSPE and MAE. Figure 9 showcases predictions at a selection of central testing

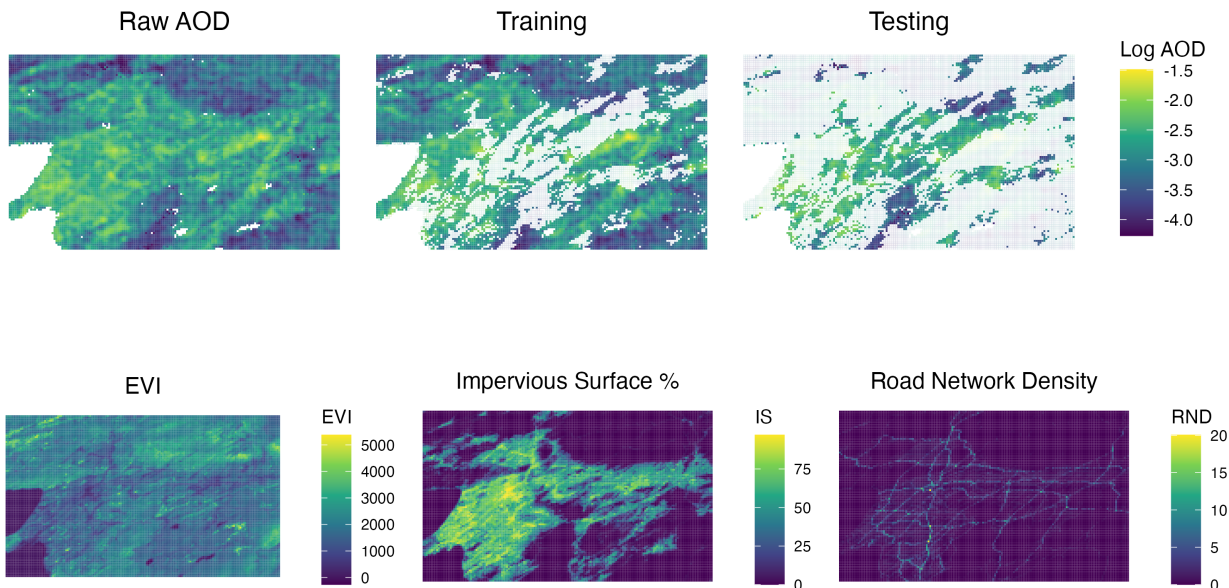


FIGURE 8. Upper: MODIS Aerosol Optical Depth (AOD) Visualization. From left to right: Log-transformed AOD values, training data (pixels not covered by clouds), and testing data (cloud-covered pixels), as of September, 13th, 2018. Lower: Visualization of Regression Model Predictors. From left to right: Enhanced Vegetation Index (EVI) from MODIS MOD13A2 products, impervious surface percentage from USGS NLCD 2018, and weighted road network density from OpenStreetMap, all resampled to 1-km resolution.

locations, where we note that the stacking algorithms produce smoother interpolations. We compare the 95% CI for the testing AOD in Figure 22 and provide the CI coverage (CIC) for 95% CI and 99% CI in Table 1. Although the BLR model achieved excellent CI coverage, the CIs it produced are remarkably wider than those obtained through stacking. This analysis demonstrates the effectiveness of our stacking algorithms in AOD interpolation, notably outperforming prevailing models in accuracy and uncertainty quantification with limited predictors, showing great potential for future remote sensing data interpolation.

7. CONCLUSION AND FUTURE WORK

We explored geostatistical inference using Bayesian stacking offering theoretical insights for inferential behavior of posterior distributions in fixed-domain or infill settings and explore inferential performance through simulations and analysis of an AOD data. The empirical

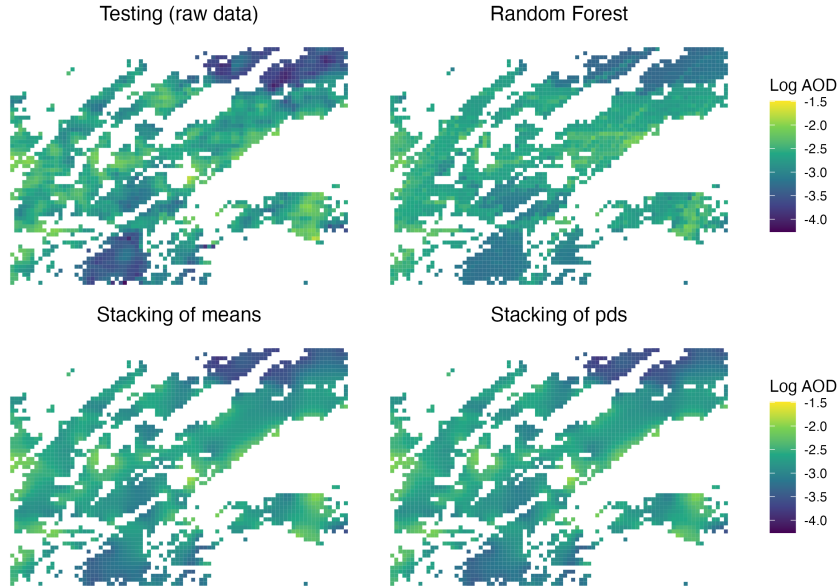


FIGURE 9. Interpolated and testing data AOD in the selected region

TABLE 1. Comparative performance metrics for AOD interpolation. Best results are in **bold**.

Method	RMSPE	MAE	R	95% CIC	99% CIC
Bayesian linear regression	0.019	0.0147	0.693	94.9%	99.4%
Deep Learning (H2O)	0.0166	0.0127	0.792	NA	NA
Gradient Boosting (H2O)	0.0161	0.0122	0.797	NA	NA
Random Forest (H2O)	0.0153	0.0115	0.821	NA	NA
Ensemble model (H2O)	0.0154	0.0116	0.816	NA	NA
Stacking of means	0.010	0.007	0.927	75.9%	87.0%
Stacking of posterior density	0.010	0.007	0.926	82.1%	93.9%

results reveal that stacking methods deliver predictions comparable to full Bayesian inference obtained using MCMC samples, but at significantly lower costs. Our proposed algorithms are implemented in parallel using efficient storage and, hence, comprise an efficient alternative to full Bayesian inference using MCMC samples. Future directions can build upon our current framework to extend Bayesian stacking for multivariate geostatistics using conjugate matrix-variate normal-Wishart families (Zhang et al., 2021) and conjugate exponential families for non-Gaussian data (Bradley et al., 2020). Stacked Bayesian inference for high-dimensional geostatistics (e.g., building on the conjugate framework in Banerjee, 2020) is also possible.

REFERENCES

- M. Abramowitz and A. Stegun. Handbook of Mathematical Functions: with Formulas, Graphs, and Mathematical Tables. Dover, 1965.
- Markus Abt. Estimating the prediction mean squared error in gaussian stochastic processes with exponential correlation structure. Scandinavian Journal of Statistics, 26(4):563–578, 1999.
- Rosana Aguilera, Nana Luo, Rupa Basu, Jun Wu, Rachel Clemesha, Alexander Gershunov, and Tarik Benmarhnia. A novel ensemble-based statistical approach to estimate daily wildfire-specific PM_{2.5} in California (2006–2020). Environment International, 171:107719, 2023.
- Erling D Andersen and Knud D Andersen. The MOSEK interior point optimizer for linear programming: an implementation of the homogeneous algorithm. In High performance optimization, pages 197–232. Springer, 2000.
- Sudipto Banerjee. Geostatistics for environmental processes. In Alan E. Gelfand, Montserrat Fuentes, Jennifer A. Hoeting, and Richard L. Smith, editors, Handbook of Environmental and Ecological Statistics, pages 81–96. CRC press, Boca Raton, FL, 2019.
- Sudipto Banerjee. Modeling massive spatial datasets using a conjugate bayesian linear modeling framework. Spatial Statistics, 37:100417, 2020.
- Sudipto Banerjee, Bradley P Carlin, and Alan E Gelfand. Hierarchical Modeling and Analysis for Spatial Data. CRC Press, Boca Raton, FL, 2014.
- James O Berger, Victor De Oliveira, and Bruno Sansó. Objective bayesian analysis of spatially correlated data. Journal of the American Statistical Association, 96(456):1361–1374, 2001. doi: 10.1198/016214501753382282. URL <https://doi.org/10.1198/016214501753382282>.
- Maitreyee Bose, James S. Hodges, and Sudipto Banerjee. Toward a diagnostic toolkit for linear models with gaussian-process distributed random effects. Biometrics, 74(3):863–873, 2018. doi: <https://doi.org/10.1111/biom.12848>. URL <https://onlinelibrary.wiley.com/doi/abs/10.1111/biom.12848>.
- Jonathan R. Bradley, Scott H. Holan, and Christopher K. Wikle. Bayesian hierarchical models with conjugate full-conditional distributions for dependent data from the natural exponential family. Journal of the American Statistical Association, 115(532):2037–2052, 2020. doi: 10.1080/01621459.2019.1677471. URL <https://doi.org/10.1080/01621459.2019.1677471>.
- Leo Breiman. Stacked regressions. Machine learning, 24(1):49–64, 1996.
- Leo Breiman. Random forests. Machine learning, 45:5–32, 2001.
- Arno Candel, Viraj Parmar, Erin LeDell, and Anisha Arora. Deep learning with h2o. H2O. ai Inc, pages 1–21, 2016.
- J. Chilés and P. Delfiner. Geostatistics: Modeling Spatial Uncertainty. John Wiley: New York, 1999.
- Merlise Clyde and Edwin S Iversen. Bayesian model averaging in the m-open framework. Bayesian theory and applications, 14(4):483–498, 2013. doi: <http://dx.doi.org/10.1093/acprof:oso/9780199695607.003.0024>.

- Darren Cook. Practical machine learning with H2O: powerful, scalable techniques for deep learning and AI. ” O’Reilly Media, Inc.”, 2016.
- N. Cressie. Statistics for Spatial Data. Wiley-Interscience, New York, revised edition, 1993.
- René de Jonge and Harry van Zanten. Semiparametric Bernstein–von Mises for the error standard deviation. Electronic Journal of Statistics, 7(none):217 – 243, 2013. doi: 10.1214/13-EJS768. URL <https://doi.org/10.1214/13-EJS768>.
- V. De Oliveira and Z Han. On information about covariance parameters in gaussian matern random fields. Journal of Agricultural, Biological and Environmental Statistics, 27:690–712, 2022.
- PJ Diggle and PJ Ribeiro. Model-based Geostatistics. Springer, 2007.
- Yulong Fan and Lin Sun. Satellite aerosol optical depth retrieval based on fully connected neural network (fcnn) and a combine algorithm of simplified aerosol retrieval algorithm and simplified and robust surface reflectance estimation (sremara). IEEE J. Sel. Top. Appl. Earth Obs., 2023.
- Andrew O Finley, Abhirup Datta, Bruce C Cook, Douglas C Morton, Hans E Andersen, and Sudipto Banerjee. Efficient algorithms for bayesian nearest neighbor gaussian processes. Journal of Computational and Graphical Statistics, 28(2):401–414, 2019.
- Jerome H Friedman. Greedy function approximation: a gradient boosting machine. Annals of statistics, pages 1189–1232, 2001.
- Marie Gaudard, Marvin Karson, Ernst Linder, and Debajyoti Sinha. Bayesian spatial prediction. Environmental and Ecological Statistics, 6(2):147–171, 1999.
- Mark S. Handcock and Michael L. Stein. A bayesian analysis of kriging. Technometrics, 35(4): 403–410, 1993. doi: 10.1080/00401706.1993.10485354. URL <https://www.tandfonline.com/doi/abs/10.1080/00401706.1993.10485354>.
- James S. Hodges. Richly Parameterized Linear Models: Additive, Time Series, and Spatial Models Using Random Effects. Chapman and Hall/CRC, Boca Raton, FL, 2013.
- Jennifer A. Hoeting, David Madigan, Adrian E. Raftery, and Chris T. Volinsky. Bayesian model averaging: a tutorial (with comments by M. Clyde, David Draper and E. I. George, and a rejoinder by the authors). Statistical Science, 14(4):382 – 417, 1999. doi: 10.1214/ss/1009212519. URL <https://doi.org/10.1214/ss/1009212519>.
- C. G. Kaufman and B. A. Shaby. The role of the range parameter for estimation and prediction in geostatistics. Biometrika, 100(2):473–484, 2013.
- Hannes Kazianka and Jürgen Pilz. Objective Bayesian analysis of spatial data with uncertain nugget and range parameters. Canadian Journal of Statistics, 40(2):304–327, 2012.
- Peter K Kitanidis. Parameter uncertainty in estimation of spatial functions: Bayesian analysis. Water resources research, 22(4):499–507, 1986.
- Tri Le and Bertrand Clarke. A bayes interpretation of stacking for m-complete and m-open settings. Bayesian Analysis, 12(3):807–829, 2017.
- Cheng Li, Saifei Sun, and Yichen Zhu. Fixed-domain posterior contraction rates for spatial gaussian process model with nugget. Journal of the American Statistical Association, 0(ja):1–21, 2023. doi: 10.1080/01621459.2023.2191380. URL <https://doi.org/10.1080/01621459.2023.2191380>.

- Z Li, X Zhao, R Kahn, M Mishchenko, L Remer, K-H Lee, M Wang, I Laszlo, T Nakajima, and H Maring. Uncertainties in satellite remote sensing of aerosols and impact on monitoring its long-term trend: a review and perspective. In Annales Geophysicae, volume 27, pages 2755–2770. Copernicus GmbH, 2009.
- Alexei Lyapustin et al. Modis collection 6 maiaac algorithm. Atmos. Meas. Tech., 11(10):5741–5765, 2018.
- David Madigan, Adrian E Raftery, C Volinsky, and Jennifer Hoeting. Bayesian model averaging. In Proceedings of the AAAI Workshop on Integrating Multiple Learned Models, Portland, OR, pages 77–83, 1996.
- Carl Edward Rasmussen and Christopher K. I. Williams. Gaussian processes for machine learning. MIT Press, Cambridge, MA, 2006.
- Paulo J Ribeiro Jr, Peter J Diggle, Maintainer Paulo J Ribeiro Jr, and MASS Suggests. The geor package. R news, 1(2):14–18, 2007.
- Michael L. Stein. Interpolation of Spatial Data: Some Theory for Kriging. Springer-Verlag, New York, 1999.
- Wenpin Tang, Lu Zhang, and Sudipto Banerjee. On identifiability and consistency of the nugget in Gaussian spatial process models. J. R. Stat. Soc. Ser. B. Stat. Methodol., 83(5):1044–1070, 2021.
- Aki Vehtari, Tommi Mononen, Ville Tolvanen, Tuomas Sivula, and Ole Winther. Bayesian leave-one-out cross-validation approximations for gaussian latent variable models. The Journal of Machine Learning Research, 17(1):3581–3618, 2016.
- Adam Voiland. Aerosols: Tiny particles, big impact. NASA Earth Observatory, 2, 2010.
- David H Wolpert. Stacked generalization. Neural networks, 5(2):241–259, 1992.
- Yuling Yao, Aki Vehtari, Daniel Simpson, and Andrew Gelman. Using stacking to average bayesian predictive distributions (with discussion). Bayesian Analysis, 13(3):917–1007, 2018.
- Yuling Yao, Aki Vehtari, and Andrew Gelman. Stacking for non-mixing bayesian computations: The curse and blessing of multimodal posteriors. arXiv:2006.12335, 2020.
- Yuling Yao, Gregor Pirεs, Aki Vehtari, and Andrew Gelman. Bayesian hierarchical stacking: Some models are (somewhere) useful. Bayesian Analysis, 1(1):1–29, 2021.
- Hao Zhang. Inconsistent estimation and asymptotically equal interpolations in model-based geostatistics. Journal of the American Statistical Association, 99(465):250–261, 2004.
- Hao Zhang and Dale L Zimmerman. Towards reconciling two asymptotic frameworks in spatial statistics. Biometrika, 92(4):921–936, 2005.
- Lu Zhang, Sudipto Banerjee, and Andrew O Finley. High-dimensional multivariate geostatistics: A Bayesian matrix-normal approach. Environmetrics, 32(4):e2675, 2021.
- Dale Zimmerman and Noel Cressie. Mean squared prediction error in the spatial linear model with estimated covariance parameters. Annals of the Institute of Statistical Mathematics, 44:27–43, 1992.
- Dale Zimmerman and Michael Stein. Classical geostatistical methods. In Alan E Gelfand, Peter Diggle, Peter Guttorp, and Montserrat Fuentes, editors, Handbook of spatial statistics, pages 29–44. CRC press, Boca Raton, FL, 2010.

APPENDIX A. PROOF OF THEOREM 3.1

Theorem 3.1. *Assume that the location set $\chi = \{s_1, \dots, s_n\}$ satisfies*

$$\max_{s \in \mathcal{D}} \min_{1 \leq i \leq n} |s - s_i| \asymp n^{-\frac{1}{d}}. \quad (3.4)$$

Let \mathbb{P}_0 be the probability distribution of the Matérn model (3.1) with $(\sigma_0^2, \phi_0, \tau_0^2)$. Under \mathbb{P}_0 ,

$$\lim_{n \rightarrow \infty} p(\sigma^2 | y(\chi)) = \text{Dirac}(\tau_0^2/\delta^2), \text{ and } \lim_{n \rightarrow \infty} p(\tau^2 | y(\chi)) = \text{Dirac}(\tau_0^2) \quad (3.5)$$

where $y(\chi) = (y(s_1), y(s_2), \dots, y(s_n))^T$, and $\text{Dirac}(\cdot)$ denotes the Dirac mass point.

The proof of this theorem breaks into the following lemmas. Recall the definition of $b_\sigma^* = b_{\sigma,n}^*$ from Lemma 2.1. We derive a simple expression for $b_{\sigma,n}^*$, which is specific to the conjugate model (3.3).

Lemma 3.2. *We have $b_{\sigma,n}^* = b_\sigma + \frac{1}{2}y(\chi)^T(\delta^2 I_n + R_\phi(\chi))^{-1}y(\chi)$.*

Proof. Note that

$$M_*^{-1} = x_*^T V_{y_*}^{-1} x_* = \delta^{-2} I_n + R_\phi(\chi) \quad \text{and} \quad m_* = x_*^T V_{y_*}^{-1} y_* = \delta^{-2} y(\chi). \quad (\text{A.1})$$

By the Woodbury matrix identity, we can simplify $m_*^T M_* m_* = \delta^{-2} y(\chi)^T (I_n + \delta^2 R_\phi^{-1}(\chi))^{-1} y(\chi)$ as

$$\delta^{-2} y(\chi)^T y(\chi) - y(\chi)^T (\delta^2 I_n + R_\phi(\chi))^{-1} y(\chi) = y_*^T V_{y_*}^{-1} y_* - y(\chi)^T (\delta^2 I_n + R_\phi(\chi))^{-1} y(\chi),$$

which yields the desired result. \square

The next lemma investigates the asymptotic behavior of b_σ^* when the range decay $\phi = \phi_0$, i.e., ϕ is fixed at the value generating the data.

Lemma 3.3. *Let $\phi = \phi_0$, and assume that $\max_{s \in \mathcal{D}} \min_{1 \leq i \leq n} |s - s_i| \asymp n^{-\frac{1}{d}}$. Then*

$$\frac{b_{\sigma,n}^* - b_\sigma}{n} \longrightarrow \frac{\tau_0^2}{2\delta^2}, \quad \mathbb{P}_0\text{-almost surely.} \quad (3.6)$$

Proof. Let Q_n be the orthogonal matrix such that $Q_n R_{\phi_0}(\chi) Q_n^\top = \begin{pmatrix} \lambda_1^{(n)} & & \\ & \ddots & \\ & & \lambda_n^{(n)} \end{pmatrix}$,

where $\lambda_i^{(n)}$ is the i -th largest eigenvalue of matrix $R_{\phi_0}(\chi)$. Thus, under \mathbb{P}_0 ,

$$Q_n y(\chi) \sim \mathcal{N} \left(0, \begin{pmatrix} \sigma_0^2 \lambda_1^{(n)} + \tau_0^2 & & \\ & \ddots & \\ & & \sigma_0^2 \lambda_n^{(n)} + \tau_0^2 \end{pmatrix} \right).$$

By Lemma 3.2, we get

$$2(b_{\sigma,n}^* - b_\sigma) = \sum_{i=1}^n \frac{\sigma_0^2 \lambda_i^{(n)} + \tau_0^2}{\lambda_i^{(n)} + \delta^2} u_i^2, \quad (\text{A.2})$$

where $u_i \stackrel{i.i.d.}{\sim} \mathcal{N}(0, 1)$ for $i = 1, \dots, n$. By Tang et al. (2021, Corollary 2), there exists $C > 0$ independent of n such that $\lambda_i^{(n)} \leq C n i^{-\frac{2\nu}{d}-1}$ for all $1 \leq i \leq n$. This implies that

$$\sum_{i=1}^n \frac{\sigma_0^2 \lambda_i^{(n)} + \tau_0^2}{\lambda_i^{(n)} + \delta^2} \sim \frac{n \tau_0^2}{\delta^2} \quad \text{as } n \rightarrow \infty. \quad (\text{A.3})$$

By the law of large numbers, (3.6) follows from (A.2) and (A.3). \square

Proof of Theorem 3.1. Let $\sigma'^2 := \sigma_0^2 \phi_0^{2\nu} / \phi^{2\nu}$, and let \mathbb{P}' be the probability distribution of the Matérn model with parameters $(\sigma'^2, \phi, \tau_0^2)$. By Tang et al. (2021, Theorem 1), \mathbb{P}' is equivalent to \mathbb{P} . Further by Lemma 3.3,

$$\frac{b_{\sigma,n}^* - b_\sigma}{n} \rightarrow \frac{\tau_0^2}{2\delta^2}, \quad \mathbb{P}'\text{-almost surely.}$$

which also holds \mathbb{P}_0 -almost surely. Now by Lemma 2.1,

$$\mathbb{E}_0(\sigma^2 | y(\chi)) = \frac{b_{\sigma,n}^*}{a_{\sigma,n}^*} \sim \frac{\tau_0^2}{\delta^2} \quad \text{and} \quad \mathbb{V}_0(\sigma^2 | y(\chi)) = \frac{b_{\sigma,n}^{*2}}{(a_{\sigma,n}^* - 1)^2 (a_{\sigma,n}^* - 2)} \asymp \frac{1}{n}, \quad (\text{A.4})$$

which yields (3.5) by Chebyshev's inequality. This implies the posterior consistency of $\tau^2 = \delta^2 \sigma^2$. \square

APPENDIX B. PROOF OF THEOREM 3.4

Theorem 3.4. *Let $s_0 \in \mathcal{D}$. For any given $\phi > 0$, denote $\text{Cov}(z, z(s_0) | \sigma^2)$ and $R_\phi(\chi)$ by $\sigma^2 J_{\phi,n}$ and $R_{\phi,n}$, respectively. Then we have the decomposition*

$$\mathbb{E}_0(Z_n(s_0) - z(s_0))^2 = E_{1,n} + E_{2,n} + o(1), \quad (\text{3.7})$$

where $E_{1,n}$ is the prediction error of the best linear predictor for a Matérn model with parameters $\{\sigma'^2, \phi, \tau'^2\}$ satisfying $\delta^2 = \frac{\tau'^2}{\sigma'^2}$, and

$$E_{2,n} := \frac{\tau_0^2}{\delta^2} [1 - J_{\phi,n}^\top (\delta^2 I_n + R_{\phi,n})^{-1} J_{\phi,n}] \quad (3.8)$$

Consequently, if $E_{1,n}, E_{2,n} \rightarrow 0$ as $n \rightarrow \infty$, then the latent process $z(s)$ is posterior predictive consistent in the sense that $\mathbb{E}_0(Z_n(s_0) - z(s_0))^2 \rightarrow 0$ as $n \rightarrow \infty$ and, hence, $\mathbb{E}_0(Y_n(s_0) - y(s_0))^2 \rightarrow 2\tau_0^2$ as $n \rightarrow \infty$.

Proof. By (A.1), we have

$$p(z | y, \sigma^2) = \mathcal{N}((I_n + \delta^2 R_\phi(\chi)^{-1})^{-1} y, \sigma^2 (\delta^{-2} I_n + R_\phi(\chi)^{-1})^{-1}).$$

Combining with (G.12), we get the posterior predictive mean

$$\begin{aligned} \mathbb{E}(z(s_0) | y_n) &= J_{\phi,n}^\top R_\phi(\chi)^{-1} \mathbb{E}(z | y_n) \\ &= J_{\phi,n}^\top R_\phi(\chi)^{-1} (I_n + \delta^2 R_\phi(\chi)^{-1})^{-1} y_n = J_{\phi,n}^\top (\delta^2 I_n + R_\phi(\chi))^{-1} y_n, \end{aligned}$$

which is the best linear predictor corresponding to a Matérn model with parameter values $\{\sigma'^2, \phi, \tau'^2\}$ satisfying $\delta^2 = \tau'^2 / \sigma'^2$. Further by Theorem 3.1, the formula (G.13) reduces to

$$\mathbb{V}(z(s_0) | y_n) \rightarrow \frac{\tau_0^2}{\delta^2} (1 - J_{\phi,n}^\top R_\phi(\chi)^{-1} J_{\phi,n}) + \tau_0^2 J_{\phi,n}^\top (\delta^2 I_n + R_\phi(\chi))^{-1} R_\phi(\chi)^{-1} J_{\phi,n},$$

which gives (3.8). The rest of the theorem easily follows. \square

APPENDIX C. PROOF OF PROPOSITION 3.6

Proposition 3.6. *Let $\mathcal{D} = [-1, 1]$ and $\chi = \{i/n, -n \leq i \leq n\}$. Under Assumption 3.5, we have $e \rightarrow 0$ as $n \rightarrow \infty$, where e is the prediction error of the best linear predictor defined as in (3.9).*

Proof. To simplify the notation, we denote by $\Delta := \frac{1}{n}$ the inter-spacing of the grid. Let f_0 (resp. f) be the spectral density of the Matérn model with true parameter values $\{\sigma_0^2, \phi_0, \tau_0^2\}$ and the smoothness parameter ν_0 (resp. possibly misspecified parameter values $\{\sigma^2, \phi, \tau^2\}$ and the smoothness parameter ν). Define

$$\tilde{f}_0^\Delta(u) = \Delta^{-1} \sum_{k=-\infty}^{\infty} f_0\left(\frac{u + 2\pi k}{\Delta}\right) \quad \text{and} \quad \tilde{f}^\Delta(u) = \Delta^{-1} \sum_{k=-\infty}^{\infty} f\left(\frac{u + 2\pi k}{\Delta}\right).$$

By (Stein, 1999, Chapter 3, (13)), the prediction error of $y(0)$ based on $y(s)$, $s \in \chi_\infty \setminus \{0\}$ is

$$4\pi^2 \int_{-\pi}^{\pi} \frac{\tilde{f}_0^\Delta(u)}{\tilde{f}^\Delta(u)^2} du \Big/ \left(\int_{-\pi}^{\pi} \tilde{f}^\Delta(u)^{-1} du \right)^2,$$

and hence the prediction error of $z(0)$ based on $y(s)$, $s \in \chi_\infty \setminus \{0\}$ is

$$e_\infty = \frac{4\pi^2 \int_{-\pi}^{\pi} \frac{\tilde{f}_0^\Delta(u)}{\tilde{f}^\Delta(u)^2} du}{\left(\int_{-\pi}^{\pi} \tilde{f}^\Delta(u)^{-1} du \right)^2} - \tau_0^2.$$

The spectral density of the Matérn model without the nugget is

$$f_{\text{Matérn}}(u) = C \frac{\sigma^2 \phi^{2\nu}}{(\phi^2 + u^2)^{\nu+d/2}} \quad \text{for some } C > 0.$$

We write

$$\tilde{f}_0^\Delta(u) = \sigma_0^2 g_0^\Delta(u) + \frac{\tau_0^2}{2\pi} \quad \text{and} \quad \tilde{f}^\Delta(u) = \sigma^2 g^\Delta(u) + \frac{\tau^2}{2\pi},$$

so that

$$e_\infty = \frac{4\pi^2 \int_{-\pi}^{\pi} \frac{\sigma_0^2 g_0^\Delta(u) + \frac{1}{2\pi} \tau_0^2}{(\sigma^2 g^\Delta(u) + \frac{1}{2\pi} \tau^2)^2} du}{\left(\int_{-\pi}^{\pi} (\sigma^2 g^\Delta(u) + \frac{1}{2\pi} \tau^2)^{-1} du \right)^2} - \tau_0^2 \quad (\text{C.1})$$

Note that $g^\Delta(u) \sim cu^{-2\nu-1}$ for some $c > 0$. It is known that (see e.g. (Tang et al., 2021, Section 2.3))

$$\int_{-\pi}^{\pi} \left(\sigma^2 g^\Delta(u) + \frac{1}{2\pi} \tau^2 \right)^{-1} du \sim \frac{4\pi^2}{\tau^2 + C\Delta^{\frac{2\nu}{2\nu+1}}} \quad \text{for some } C > 0. \quad (\text{C.2})$$

Furthermore, $g^\Delta(u) \asymp \Delta^{2\nu}$ for u large and $g^\Delta(u) \asymp \Delta^{-1}$ for u small. We prove that $e_\infty \rightarrow 0$ as $n \rightarrow \infty$. Further by Assumption 3.5, we get $e \rightarrow 0$ as $n \rightarrow \infty$. Therefore,

$$\int_{-\pi}^{\pi} \frac{\sigma_0^2 g_0^\Delta(u) + \frac{1}{2\pi} \tau_0^2}{(\sigma^2 g^\Delta(u) + \frac{1}{2\pi} \tau^2)^2} du = \frac{4\pi^2 \tau_0^2}{\tau^4} + \mathcal{O}(\Delta^{\min(2\nu_0, 2\nu, 1)}). \quad (\text{C.3})$$

Combining (C.1), (C.2) and (C.3) yields

$$e_\infty = \left(\tau_0^2 + \mathcal{O}(\Delta^{\min(2\nu_0, 2\nu, 1)}) \right) \left(1 + \frac{C\Delta^{\frac{2\nu}{2\nu+1}}}{\tau^2} \right) - \tau_0^2 \asymp \Delta^{\min(2\nu_0, \frac{2\nu}{2\nu+1})}.$$

Thus, we have $e_\infty \rightarrow 0$ as $n \rightarrow \infty$, and by Assumption 3.5 we obtain the result in Proposition 3.6. \square

APPENDIX D. PROOF OF PROPOSITION 3.7

Proposition 3.7. *Let $s_0 \in \mathcal{D}$, and $w^* := (w_1^*, \dots, w_G^*)$ be the stacking weights (e.g. defined by (2.6)) such that $|w_g^*|$ is bounded for each $1 \leq g \leq G$. Let the assumptions in Theorem 3.4 or Theorem G.2 hold for each model M_g . We have*

$$\mathbb{E}_0 \left(y(s_0) - \sum_{g=1}^G w_g^* \mathbb{E}_g(y(s_0) | y) \right)^2 \rightarrow \tau_0^2 \quad \text{as } n \rightarrow \infty. \quad (3.10)$$

Proof. For ease of presentation, we give the proof in the setting of Theorem 3.4. Note that

$$\begin{aligned} \mathbb{E}_0 \left(y(s_0) - \sum_{g=1}^G w_g^* \mathbb{E}_g(y(s_0) | y) \right)^2 &= \tau_0^2 + \mathbb{E}_0 \left(\sum_{g=1}^G w_g^* (z(s_0) - \mathbb{E}_g(z(s_0) | y)) \right)^2 \\ &\leq \tau_0^2 + \sum_{g=1}^G w_g^{*2} \sum_{g=1}^G \mathbb{E}_0 (z(s_0) - \mathbb{E}_g(z(s_0) | y))^2, \end{aligned} \quad (D.1)$$

where we apply the Cauchy-Schwarz inequality in (D.1). For each $1 \leq g \leq G$, $\mathbb{E}_0 (z(s_0) - \mathbb{E}_g(z(s_0) | y))^2$ corresponds to the deviation error $E_{1,n}$ for the model M_g , which goes to 0 as $n \rightarrow \infty$. Since $|w_g^*|$ is bounded for each g , the bound (3.10) follows readily from (D.1). \square

APPENDIX E. PROOF OF THEOREM 3.8

Theorem 3.8. *Let $s_0 \in \mathcal{D}$, and $w^* := (w_1^*, \dots, w_G^*)$ be the stacking weights (e.g. defined by (2.6)) such that $|w_g^*|$ is bounded for each $1 \leq g \leq G$. Let*

$$E_{1,g,i} := \mathbb{E}_0 (z(s_i) - \hat{y}_g(s_i))^2, \quad 1 \leq g \leq G \text{ and } 1 \leq i \leq n,$$

be the deviation error for the latent process $z(s)$ by leaving the i^{th} observation out under the model M_g . Assume that for each $1 \leq g \leq G$,

$$\frac{1}{n} \sum_{i=1}^n E_{1,g,i} \rightarrow 0 \quad \text{as } n \rightarrow \infty. \quad (3.11)$$

Also let the assumptions in Theorem G.2 or Theorem 3.4 hold for each model M_g . We have as $n \rightarrow \infty$,

$$\mathbb{E}_0 \left(y(s_0) - \sum_{g=1}^G w_g^* \mathbb{E}_g(y(s_0) | y) \right)^2 - \mathbb{E}_0 \left(\frac{1}{n} \sum_{i=1}^n \left(y(s_i) - \sum_{g=1}^G w_g^* \hat{y}_g(s_i) \right)^2 \right) \rightarrow 0. \quad (3.12)$$

Proof. By Proposition 3.7, it suffices to prove that

$$\mathbb{E}_0 \left(\frac{1}{n} \sum_{i=1}^n \left(y(s_i) - \sum_{g=1}^G w_g^* \hat{y}_g(s_i) \right)^2 \right) \rightarrow \tau_0^2 \quad \text{as } n \rightarrow \infty. \quad (\text{E.1})$$

For ease of presentation, we prove (E.1) in the setting of Theorem 3.4. Note that

$$\begin{aligned} \mathbb{E}_0 \left(\frac{1}{n} \sum_{i=1}^n \left(y(s_i) - \sum_{g=1}^G w_g \hat{y}_g(s_i) \right)^2 \right) &= \tau_0^2 + \underbrace{\frac{1}{n} \mathbb{E}_0 \sum_{i=1}^n \left(\sum_{g=1}^G w_g^* (z(s_i) - \hat{y}_g(s_i)) \right)^2}_B \\ &\leq \tau_0^2 + \frac{1}{n} \sum_{g=1}^G w_g^{*2} \sum_{i=1}^n E_{1,g,i}. \end{aligned} \quad (\text{E.2})$$

By the boundedness of $|w_g^*|$ and the condition (3.11), the limit (E.1) follows easily from (E.2). \square

Taking a closer look at (E.2), we can see that B summarises the average squared prediction errors for $z(s_i), i = 1, \dots, n$, in a LOO cross-validation. Hence, the stacking weights obtained from (2.6) minimises the average squared prediction errors for the latent process over the observed locations.

APPENDIX F. PROOF OF THEOREM 3.10

Theorem 3.10. *Let \mathbb{P}_0 be the probability measure of the model (2.1) with parameter values $\{\beta_0, \sigma_0^2, \Phi_0, \tau_0^2\}$, and let Assumption 3.9 hold. Let $H = X_{\dagger}(X_{\dagger}^T X_{\dagger})^{-1} X_{\dagger}^T$ be the $(2n + p) \times (2n + p)$ orthogonal projector onto the column space of X_{\dagger} and let $H = \begin{pmatrix} H_{11} & H_{12} \\ H_{12}^T & H_{22} \end{pmatrix}$ be a 2×2 partition of H so that H_{22} is the lower right $n \times n$ block formed by rows and columns indexed from $n + p + 1$ to $2n + p$. Assume that $\text{Tr}(H_{22})/n \rightarrow \alpha$ as $n \rightarrow \infty$. Then under \mathbb{P}_0 ,*

$$\lim_{n \rightarrow \infty} p(\sigma^2 | y(\chi)) = \text{Dirac}(\sigma_{\alpha}^2), \quad (3.14)$$

where $\sigma_{\alpha}^2 := \frac{\tau_0^2}{\delta^2} \alpha + \sigma'^2(1 - \alpha)$.

Proof. For ease of presentation, we denote $y(\chi)$ by y_n in the proofs. By Assumption 3.9, there is a probability distribution $\mathbb{P}' \equiv \mathbb{P}_0$, which corresponds to the model with parameters $(\beta_0, \sigma'^2, \Phi, \tau_0^2)$ for some σ'^2 . Under \mathbb{P}' , there exists a γ_0 such that

$$y_{\dagger} - X_{\dagger} \gamma_0 | \sigma^2 \sim \mathcal{N}(0, V'), \quad (\text{F.1})$$

where $V' = \begin{pmatrix} \frac{\tau_0^2}{\delta^2} I_n & 0 & 0 \\ 0 & \sigma^2 I_p & 0 \\ 0 & 0 & \sigma'^2 I_n \end{pmatrix}$. Consider the sequence $\zeta_n \sim p(\sigma^2 | y_n)$. Under \mathbb{P}' , $\zeta_n \sim IG(a_{\sigma,n}^*, b_{\sigma,n}^*)$, where $a_{\sigma,n}^* = a_\sigma + n/2$ and

$$\begin{aligned} b_{\sigma,n}^* &= b_\sigma + \frac{1}{2} (y_\dagger - X_\dagger \gamma_0)^\top (I_{2n+p} - H) (y_\dagger - X_\dagger \gamma_0) \\ &= b_\sigma + \frac{1}{2} [Q(y_\dagger - X_\dagger \gamma_0)]^\top \begin{pmatrix} 0 & 0 \\ 0 & I_n \end{pmatrix} [Q(y_\dagger - X_\dagger \gamma_0)], \end{aligned} \quad (\text{F.2})$$

The expectation under \mathbb{P}' for $b_{\sigma,n}^*$ is

$$\begin{aligned} \mathbb{E}'(b_{\sigma,n}) &= b_\sigma + \frac{1}{2} \mathbb{E}'(y_\dagger^\top (I_{2n+p} - H) y_\dagger) \\ &= b_\sigma + \frac{1}{2} \left\{ \gamma_0^\top X_\dagger^\top (I_{2n+p} - H) X_\dagger \gamma_0 + \text{Tr}((I_{2n+p} - H) V') \right\} \\ &= b_\sigma + \frac{1}{2} \text{Tr}((I_{2n+p} - H) V') \quad (\text{since } (I_{2n+p} - H) X_\dagger = O) \\ &= b_\sigma + \frac{1}{2} \text{Tr} \left(Q_{21}^\top Q_{21} \begin{pmatrix} \frac{\tau_0^2}{\delta^2} I_n & O \\ O & \sigma^2 I_p \end{pmatrix} \right) + \frac{\sigma'^2}{2} \text{Tr}(Q_{22}^\top Q_{22}), \end{aligned} \quad (\text{F.3})$$

where $Q = \begin{pmatrix} Q_{11} & Q_{12} \\ Q_{21} & Q_{22} \end{pmatrix}$ is an orthogonal matrix such that $H = Q^\top \begin{pmatrix} I_{n+p} & 0 \\ 0 & 0 \end{pmatrix} Q$ with Q_{22} being the lower right $n \times n$ block of Q in a 2×2 partition. Using $Q_{21} Q_{21}^\top = I_n - Q_{22} Q_{22}^\top$ and some further simplification we obtain

$$\mathbb{E}'(b_{\sigma,n}^*) = b_\sigma + \frac{n}{2} \left(\frac{\tau_0^2}{\delta^2} (1 - \text{Tr}(Q_{22}^\top Q_{22}/n)) + \sigma'^2 \text{Tr}(Q_{22}^\top Q_{22}/n) \right) + \underbrace{\frac{p}{2} \left(\sigma^2 - \frac{\tau_0^2}{\delta^2} \right)}_{o(n)}. \quad (\text{F.4})$$

Since $\mathbb{E}'(\zeta_n) = \mathbb{E}'(b_{\sigma,n}^*) / (a_{\sigma,n}^* - 1)$ and $\text{Tr}(Q_{22}^\top Q_{22}) = n - \text{Tr}(H_{22})$, where $\text{Tr}(H_{22})/n \rightarrow \alpha$ as $n \rightarrow \infty$, we obtain $\lim_{n \rightarrow \infty} \mathbb{E}'(\zeta_n) = \sigma_\alpha^2$. The variance of ζ_n under \mathbb{P}' is given by

$$\begin{aligned} \mathbb{V}'(\zeta_n) &= \mathbb{E}'[\mathbb{V}(\zeta_n | y_n)] + \mathbb{V}'[\mathbb{E}(\zeta_n | y_n)] \\ &= \mathbb{E}' \left(\frac{b_{\sigma,n}^{*2}}{(a_{\sigma,n}^* - 1)^2 (a_{\sigma,n}^* - 2)} \right) + \mathbb{V}' \left(\frac{b_{\sigma,n}^*}{a_{\sigma,n}^* - 1} \right). \end{aligned} \quad (\text{F.5})$$

Further note that

$$\begin{aligned} \mathbb{V}'(b_{\sigma,n}^*) &= \frac{3}{4} \text{Tr} \left[\left(\frac{\tau_0^2}{\delta^2} (I_n - Q_{22}^\top Q_{22}) + \sigma'^2 Q_{22}^\top Q_{22} \right)^2 \right] + o(n) \\ &\leq C (n + \text{Tr}(Q_{22}^\top Q_{22}) + \text{Tr}[(Q_{22}^\top Q_{22})^2]), \end{aligned} \quad (\text{F.6})$$

for some $C > 0$ independent of n . Since $Q_{21}Q_{21}^\top + Q_{22}Q_{22}^\top = I_n$, we have $\text{Tr}(Q_{22}^\top Q_{22})$ and $\text{Tr}[(Q_{22}^\top Q_{22})^2]$ are bounded from above by n . Hence,

$$\frac{\mathbb{V}'(b_{\sigma,n}^*)}{n^2} \rightarrow 0 \quad \text{and} \quad \frac{\mathbb{E}'(b_{\sigma,n}^{*2})}{n^{2+\kappa}} \rightarrow 0 \quad \text{for any } \kappa > 0. \quad (\text{F.7})$$

Combining (F.5) and (F.7) yields $\lim_{n \rightarrow \infty} \mathbb{V}'(\zeta_n) = 0$. By Chebyshev's inequality, ζ_n converges in probability under \mathbb{P}' , and hence under \mathbb{P}_0 , to σ_α^2 . \square

APPENDIX G. PREDICTIVE CONSISTENCY FOR GENERAL CONJUGATE SPATIAL MODELS

Corollary G.1. *Let \mathbb{P}_0 be the probability distribution in (2.1) with parameters $\{\beta_0, \sigma_0^2, \Phi_0, \tau_0^2\}$. Define $U = (X_\dagger^\top X_\dagger)^{-1} = \begin{pmatrix} U_{11} & U_{12} \\ U_{12}^\top & U_{22} \end{pmatrix}$, where U_{11} is $p \times p$, $B = U \begin{pmatrix} X^\top X & X^\top \\ X & I_n \end{pmatrix} U = \begin{pmatrix} B_{11} & B_{12} \\ B_{21} & B_{22} \end{pmatrix}$, where B_{11} is $p \times p$, $C = U_{11}V_\beta^{-1}U_{11}$, and $D = U_{12}R_\Phi(\chi)^{-1}U_{12}^\top$. Let Assumption 3.9 hold and assume the following additional conditions:*

$$\text{Tr}(U_{11}), \text{Tr}(B_{11}), \text{Tr}(C), \text{Tr}(D) \longrightarrow 0 \quad \text{as } n \rightarrow \infty. \quad (\text{G.1})$$

Then, $\lim_{n \rightarrow \infty} p(\beta | y(\chi)) = \text{Dirac}(\beta_0)$ under \mathbb{P}_0 .

Proof. Again we denote $y(\chi)$ by y_n . The conditional posterior distribution $p(\beta | \sigma^2, y_n)$ is derived from Lemma 2.1 as $\mathcal{N}(\beta | (M_* m_*)_{[1:p]}, \sigma^2 (M_*)_{[1:p,1:p]})$, where $M_*^{-1} = V_\beta^{-1} + X^\top (R_\Phi(\chi) + \delta^2 I_n)^{-1} X$ and $m_* = V_\beta^{-1} \mu_\beta + X^\top (\delta^2 R_\Phi(\chi) + I_n)^{-1} y_n$. Let $\xi_n \sim p(\beta | y_n)$. Straightforward algebra yields

$$\mathbb{E}' \|\xi_n - \beta_0\|^2 = \frac{\tau_0^2}{\delta^4} \text{Tr}(B_{11}) + \mathbb{E}'(\zeta_n) \text{Tr}(C) + \sigma'^2 \text{Tr}(D) + \mathbb{E}'(\zeta_n) \text{Tr}(U_{11}). \quad (\text{G.2})$$

Since $\mathbb{E}'(\zeta_n) \rightarrow \sigma_\alpha^2 < \infty$ from Theorem 3.10, the proof follows from (G.1) and (G.2). \square

Derivation of (G.2).

$$\begin{aligned}
\mathbb{E}' \|\xi_n - \beta_0\|^2 &= \mathbb{E}' [\mathbb{E}' \{(\xi_n - \beta_0)^\top (\xi_n - \beta_0) \mid y_n\}] \\
&= \mathbb{E}' [\mathbb{E}' \{(\xi_n - \mathbb{E}'(\xi_n \mid y_n) + \mathbb{E}'(\xi_n \mid y_n) - \beta_0)^\top (\xi_n - \mathbb{E}'(\xi_n \mid y_n) + \mathbb{E}'(\xi_n \mid y_n) - \beta_0) \mid y_n\}] \\
&= \mathbb{E}' [\mathbb{E}' \{(\xi_n - \mathbb{E}'(\xi_n \mid y_n))^\top (\xi_n - \mathbb{E}'(\xi_n \mid y_n)) \mid y_n\}] \\
&\quad + 2\mathbb{E}' \left[\mathbb{E}' \left\{ (\mathbb{E}'(\xi_n \mid y_n) - \beta_0)^\top \underbrace{(\xi_n - \mathbb{E}'(\xi_n \mid y_n))}_{=0} \mid y_n \right\} \right] \\
&\quad + \mathbb{E}' [\mathbb{E}' \{(\mathbb{E}'(\xi_n \mid y_n) - \beta_0)^\top (\mathbb{E}'(\xi_n \mid y_n) - \beta_0) \mid y_n\}] \\
&= \mathbb{E}' [\text{Tr}\{\mathbb{V}'(\xi_n \mid y_n)\}] + \mathbb{E}' [(\mathbb{E}'(\xi_n \mid y_n) - \beta_0)^\top (\mathbb{E}'(\xi_n \mid y_n) - \beta_0)] \tag{G.3}
\end{aligned}$$

Let $\zeta_n \sim p(\sigma^2 \mid y_n)$. By the definition of ξ_n , we have

$$\begin{aligned}
\mathbb{V}'(\xi_n \mid y_n) &= \mathbb{V}'[\mathbb{E}'(\beta \mid \sigma^2, y_n) \mid y_n] + \mathbb{E}'(\mathbb{V}'[\beta \mid \sigma^2, y_n] \mid y_n) \\
&= \underbrace{\mathbb{V}'[(M_* m_*)_{[1:p]} \mid y_n]}_{=0} + \mathbb{E}'(\sigma^2 (M_*)_{[1:p],[1:p]} \mid y_n) \\
&= \mathbb{E}'(\zeta_n \mid y_n) (M_*)_{[1:p],[1:p]} = \mathbb{E}'(\zeta_n \mid y_n) U_{11}, \tag{G.4} \\
\mathbb{E}'(\xi_n \mid y_n) &= \mathbb{E}'\{\mathbb{E}'(\beta \mid \sigma^2, y_n) \mid y_n\} = (M_* m_*)_{[1:p]}.
\end{aligned}$$

With $M_* = (X_\dagger^\top X_\dagger)^{-1} = U$, $m_* = X_\dagger^\top y_\dagger$, under \mathbb{P}' ,

$$\begin{aligned}
(M_* m_*)_{[1:p]} \mid \sigma^2 &\sim \mathcal{N}(\beta_0, [M_* X_\dagger^\top V' X_\dagger M_*]_{[1:p],[1:p]}) \\
&\sim \mathcal{N}\left(\beta_0, \left[U \begin{pmatrix} \frac{\tau_0^2}{\delta^4} X^\top X + \sigma^2 V_\beta^{-1} & \frac{\tau_0^2}{\delta^4} X^\top \\ \frac{\tau_0^2}{\delta^4} X & \frac{\tau_0^2}{\delta^4} I_n + \sigma'^2 R_\Phi^{-1}(\chi) \end{pmatrix} U \right]_{[1:p],[1:p]} \right). \tag{G.5}
\end{aligned}$$

Therefore, $\mathbb{E}'[\mathbb{E}'(\xi_n \mid y_n)] = \beta_0$, and

$$\begin{aligned}
&\mathbb{E}' [(\mathbb{E}'(\xi_n \mid y_n) - \beta_0)^\top (\mathbb{E}'(\xi_n \mid y_n) - \beta_0)] \\
&= \text{Tr}\{\mathbb{V}'[\mathbb{E}'(\xi_n \mid y_n)]\} \\
&= \text{Tr}\{\mathbb{V}'[(M_* m_*)_{[1:p]}]\} \tag{G.6} \\
&= \text{Tr}\{\underbrace{\mathbb{V}'[\mathbb{E}'((M_* m_*)_{[1:p]} \mid \sigma^2)]}_{=0} + \mathbb{E}'(\mathbb{V}'[(M_* m_*)_{[1:p]} \mid \sigma^2])\}
\end{aligned}$$

We separate the variance $\mathbb{V}'[(M_* m_*)_{[1:p]} \mid \sigma^2]$ as presented in (G.5) into the following three parts

$$\underbrace{\frac{\tau_0^2}{\delta^4} \left[U \begin{pmatrix} X^\top X & X^\top \\ X & I_n \end{pmatrix} U \right]_{[1:p],[1:p]}}_{B_{11}} + \sigma^2 \underbrace{\left[U \begin{pmatrix} V_\beta^{-1} & 0 \\ 0 & 0 \end{pmatrix} U \right]_{[1:p],[1:p]}}_C + \sigma'^2 \underbrace{\left[U \begin{pmatrix} 0 & 0 \\ 0 & R_\Phi^{-1}(\chi) \end{pmatrix} U \right]_{[1:p],[1:p]}}_D.$$

Then

$$\mathbb{E}' [(\mathbb{E}'(\xi_n | y_n) - \beta_0)^\top (\mathbb{E}'(\xi_n | y_n) - \beta_0)] = \frac{\tau_0^2}{\delta^4} \text{Tr}(B_{11}) + \mathbb{E}'(\zeta_n) \text{Tr}(C) + \sigma'^2 \text{Tr}(D). \quad (\text{G.7})$$

Together with (G.3), (G.4), we can obtain (G.2).

Recall that $Z_n(s_0)$ is distributed as $p(z(s_0) | y(\chi))$, and $Y_n(s_0)$ is distributed as $p(y(s_0) | y(\chi))$ under \mathbb{P}_0 . Let X_{\dagger} and y_{\dagger} be defined by (3.13) and U be as in Corollary G.1. The following theorem generalizes Theorem 3.4.

Theorem G.2. *Let $s_0 \in \mathcal{D}$. For any given Φ , denote $\text{Cov}(z, z(s_0) | \sigma^2)$ and $R_{\Phi}(\chi)$ by $\sigma^2 J_{\Phi, n}$ and $R_{\Phi, n}$, respectively.*

$$\begin{aligned} F_n &= J_{\Phi, n}^\top R_{\Phi, n}^{-1} (U X_{\dagger}^\top y_{\dagger})_{[p+1:p+n]} \quad \text{and} \\ G_n &= 1 - J_{\Phi, n}^\top R_{\Phi, n}^{-1} (R_{\Phi, n} + U_{[p+1:p+n, p+1:p+n]}) R_{\Phi, n}^{-1} J_{\Phi, n}, \end{aligned}$$

Under the assumptions in Theorem 3.10, we have the decomposition (3.7), where $E_{1, n} = \mathbb{E}_0(z(s_0) - F_n)^2$ and $E_{2, n} = \sigma_\alpha^2 G_n$. Consequently, if $E_{1, n}, E_{2, n} \rightarrow 0$ as $n \rightarrow \infty$, then posterior inference for the latent process is consistent in the sense that $\mathbb{E}_0(Z_n(s_0) - z(s_0))^2 \rightarrow 0$ as $n \rightarrow \infty$, while posterior predictive inference for $y(s_0)$ satisfies

$$\mathbb{E}_0(Y_n(s_0) - y(s_0))^2 \rightarrow \tau_0^2 + \delta^2 \sigma_\alpha^2 \quad \text{as } n \rightarrow \infty. \quad (\text{G.8})$$

Proof. For ease of presentation, we denote $y(\chi)$ by y_n . Observe that

$$\begin{aligned} \mathbb{E}_0(Z_n(s_0) - z(s_0))^2 &= \mathbb{E}_0 \{Z_n(s_0) - \mathbb{E}(z(s_0) | y_n) + \mathbb{E}(z(s_0) | y_n) - z(s_0)\}^2 \\ &= \mathbb{E}_0 \{z(s_0) - \mathbb{E}(z(s_0) | y_n)\}^2 + \mathbb{E}_0 \{\mathbb{V}(z(s_0) | y_n)\}, \end{aligned} \quad (\text{G.9})$$

where the second equality follows from the fact that $z(s_0) - \mathbb{E}(z(s_0) | y_n)$ is independent of y_n . Note that

$$p(z(s_0) | y_n) = \int p(z(s_0) | y_n, \sigma^2, \gamma) \times p(\gamma | y_n, \sigma^2) \times p(\sigma^2 | y_n) d\sigma^2 d\gamma. \quad (\text{G.10})$$

By standard Gaussian conditioning (see e.g. (Rasmussen and Williams, 2006, Section 2.2)),

$$p(z(s_0) | y_n, \sigma^2, \gamma) = \mathcal{N}(J_{\Phi, n}^\top R_{\Phi, n}^{-1} z, \sigma^2 (1 - J_{\Phi, n}^\top R_{\Phi, n}^{-1} J_{\Phi, n})). \quad (\text{G.11})$$

By (G.10), (G.11) and Lemma 2.1, the posterior predictive mean is

$$\mathbb{E}(z(s_0) | y_n) = F_n. \quad (\text{G.12})$$

Further by the law of total variance and Theorem 3.10, we get

$$\begin{aligned} \mathbb{V}(z(s_0) | y_n) &= \mathbb{E}\{\mathbb{V}(z(s_0) | y_n, \sigma^2, \gamma)\} + \mathbb{V}\{\mathbb{E}(z(s_0) | y_n, \sigma^2, \gamma)\} \\ &\rightarrow \sigma_\alpha^2 (1 - J_{\Phi, n}^\top R_{\Phi, n}^{-1} J_{\Phi, n}) + \sigma_\alpha^2 J_{\Phi, n}^\top R_{\Phi, n}^{-1} U_{[p+1:p+n, p+1:p+n]} R_{\Phi, n}^{-1} J_{\Phi, n} = \sigma_\alpha^2 G_n. \end{aligned} \quad (\text{G.13})$$

Combining (G.9), (G.12) and (G.13) yields the decomposition (3.7), and hence the posterior predictive consistency for $z(s_0)$ holds if $E_{1, n}, E_{2, n} \rightarrow 0$ as $n \rightarrow \infty$.

Further, let ξ_n have the density $p(\beta | y_n)$. Under conditions (G.1), by Corollary G.1 we have $\mathbb{E}_0 \|\xi_n - \beta_0\|^2 \rightarrow 0$ as $n \rightarrow \infty$. As a result,

$$\mathbb{E}_0(Y_n(s_0) - y(s_0))^2 = \mathbb{E}_0(x(s_0)^\top(\xi_n - \beta_0))^2 + E_{1,n} + E_{2,n} + \tau_0^2 + \delta^2 \mathbb{E}_0(\sigma^2 | y_n),$$

which clearly converges to $\tau_0^2 + \delta^2 \sigma_\alpha^2$ as $n \rightarrow \infty$. \square

APPENDIX H. KL BOUND FOR STACKING OF PREDICTIVE DENSITIES

Let $y = (y(s_1), \dots, y(s_n))^\top$ be sampled from a model \mathcal{M}_0 . Given y , define the probability measure $Q_{0,y}(y') := \prod_{i=1}^n p(Y(s_i) = y'_i | y_{-i}, \mathcal{M}_0)$, where $y' = (y'_1, \dots, y'_n)$ and $Y = (Y(s_1), \dots, Y(s_n))^\top$ are random variables following \mathcal{M}_0 . Let $Q_0(\cdot) := \mathbb{E}_0(Q_{0,y}(\cdot))$, where \mathbb{E}_0 denotes expectation over $y \sim \mathcal{M}_0$. The probability distribution $Q_0(\cdot)$ can be viewed as the in-sample predictor of the distribution of y under \mathcal{M}_0 . We establish the KL bound for in-sample predictions using stacking of predictive densities.

Proposition H.1. *Define $P_{w,y}(y') := \prod_{i=1}^n \left(\sum_{g=1}^G w_g p(Y(s_i) = y'_i | y_{-i}, \mathcal{M}_g) \right)$ for any set of stacking weights $w = (w_1, \dots, w_G)$ and fixed y , where $Y(s_i) \stackrel{\text{ind}}{\sim} P_{y(s_i) | y_{-i}, \mathcal{M}_0}(\cdot)$. Let $P_w(\cdot) := \mathbb{E}_0(P_{w,y}(\cdot))$, where \mathbb{E}_0 denotes expectation with respect to $y \sim \mathcal{M}_0$. For the stacking weights with $w_g = 1$, we abbreviate $P_w(y)$ with $P_g(y)$. Let $w^* := (w_1^*, \dots, w_G^*)$ be the stacking weights defined in (2.7). Then we have*

$$KL(Q_0, P_{w^*}) \leq \sum_{g=1}^G w_g^* KL(Q_0, P_g). \quad (\text{H.1})$$

where $KL(\cdot, \cdot)$ is the KL divergence between two distributions.

Proof. Note that for any stacking weights $w = (w_1, \dots, w_G)$ and y , we have

$$\begin{aligned} \log P_{w,y}(y') &= \sum_{i=1}^n \log \left(\sum_{g=1}^G w_g p(Y(s_i) = y'_i | y_{-i}, M_g) \right) \geq \sum_{g=1}^G w_g \log \left(\prod_{i=1}^n p(Y(s_i) = y'_i | y_{-i}, M_g) \right) \\ &=: \sum_{g=1}^G w_g \log P_{g,y}(y'), \end{aligned}$$

by the concavity of the logarithmic function, where $P_{g,y}(y') = \prod_{i=1}^n p(Y(s_i) = y'_i | y_{-i}, M_g)$. Consequently,

$$\log Q_{0,y}(y') - \log P_{w,y}(y') \leq \sum_{g=1}^G w_g (\log Q_{0,y}(y') - \log P_{g,y}(y')). \quad (\text{H.2})$$

Taking expectations of both sides of (H.2) with respect to $Q_0(\cdot)$ yields $KL(Q_{0,y}, P_{w,y}) \leq \sum_{g=1}^G w_g KL(Q_{0,y}, P_{g,y})$. By the chain rule of the KL divergence, and specializing to $w = w^*$ yields (H.1). \square

APPENDIX I. DERIVE THE CLOSED FORM OF POINT-WISE PREDICTIVE DENSITY

In this subsection, we derive the posterior predictive density of the outcome $y(s_0)$ on location s_0 . We follow the notations in Section 2. First, we know that $y(s_0) | \gamma, \sigma^2, y, \Phi$ follows a Gaussian with mean $x(s_0)\beta + J_\Phi(s_0, \chi)R_\Phi^{-1}(\chi)z$ and variance $\delta^2\sigma^2$. Since the conditional posterior distribution $\gamma | \sigma^2, y, \Phi$ follows $N(M_*m_*, \sigma^2M_*)$, the conditional posterior distribution $y(s_0) | \sigma^2, y, \Phi$ still follows a Gaussian $N(\mu_{s_0}, \sigma^2V_{s_0})$ where

$$\mu_{s_0} = \underbrace{\begin{bmatrix} x(s_0) & J_\Phi(s_0, \chi)R_\Phi^{-1}(\chi) \end{bmatrix}}_{h_g^\top} M_*m_*, \quad V_{s_0} = h_g^\top M_* h_g + \delta^2.$$

Next, through equation (2.3)

$$\begin{aligned} p(y(s_0) | y, \Phi) &= \int p(y(s_0) | \sigma^2, y, \Phi) p(\sigma^2 | \Phi, y) d\sigma^2 \\ &= \int N(\mu_{s_0}, \sigma^2V_{s_0}) \text{IG}(a_*, b_*) d\sigma^2 \\ &= \int \frac{1}{(2\pi V_{s_0} \sigma^2)^{1/2}} \exp\left\{-\frac{(y(s_0) - \mu_{s_0})^2}{2\sigma^2 V_{s_0}}\right\} \frac{b_*^{a_*}}{\Gamma(a_*)} \sigma^{2(-a_*-1)} \exp\left\{-\frac{b_*}{\sigma^2}\right\} d\sigma^2 \\ &= \frac{b_*^{a_*}}{(2\pi V_{s_0})^{1/2} \Gamma(a_*)} \int \sigma^{2(-a_*-1/2-1)} \exp\left\{-\frac{1}{\sigma^2} \left(b_* + \frac{(y(s_0) - \mu_{s_0})^2}{2V_{s_0}}\right)\right\} d\sigma^2 \\ &= \frac{\Gamma(a_* + 1/2) b_*^{a_*}}{(2\pi V_{s_0})^{1/2} \Gamma(a_*)} \left(b_* + \frac{(y(s_0) - \mu_{s_0})^2}{2V_{s_0}}\right)^{-(a_*+1/2)} \end{aligned}$$

The log point-wise predictive density is

$$\begin{aligned} lp(y(s_0) | y, \Phi) &= -0.5 \log(2\pi V_{s_0}) + a_* \log b_* - (a_* + 1/2) \log\left(b_* + \frac{(y(s_0) - \mu_{s_0})^2}{2V_{s_0}}\right) \\ &\quad + \log \Gamma(a_* + 1/2) - \log \Gamma(a_*) \end{aligned} \quad (\text{I.1})$$

APPENDIX J. STACKING OF PREDICTIVE DENSITIES ALGORITHM (MONTE CARLO VERSION)

We present a Monte Carlo algorithm to estimate the log of point-wise predictive density for outcome in fold k given observations not in fold k . For each k , we generate J posterior samples of σ^2 and $(\beta^\top, z^\top)^\top = \gamma$, (i.e., $\{\sigma^{2(j)}, \gamma^{(j)}\}$ for $j = 1, \dots, J$), using data not in fold k . Then we calculate the corresponding expected outcome for location s in fold k , $\hat{y}_{(\phi, \nu, \delta^2)}^{k,j}(s)$ for $j = 1, \dots, J$. Next, we compute the predictive density of $y(s)$ conditional on the prediction $\hat{y}_{(\phi, \nu, \delta^2)}^{k,j}(s)$ and the nugget (variance of the noise process, which equals the product of δ^2 and the j -th posterior sample $\sigma^{2(j)}$) for each j . The conditional predictive distribution of $y(s)$ follows

$$p(y(s) | \sigma^{2(j)}, \gamma^{(j)}) = N(y(s) | y_{(\phi, \nu, \delta^2)}^{k,j}, \delta^2 \sigma^{2(j)}). \quad (\text{J.1})$$

Finally, the log point-wise predictive density (LPD) of $y(s)$ at location s is estimated by

$$\begin{aligned} lp_{(\phi, \nu, \delta^2)}(s) &= \log \int_{\sigma^2, \gamma} p(y(s) | \sigma^2, \gamma) p(\sigma^2, \gamma | y[-k]) d\sigma^2 d\gamma \\ &\approx \log \left\{ \frac{1}{J} \sum_{j=1}^J p_{(\phi, \nu, \delta^2)}(y(s) | \sigma^{2(j)}, \gamma^{(j)}) \right\}, \end{aligned} \quad (\text{J.2})$$

and we can compute the stacking weights based on the estimated LPDs. The following is the Monte Carlo version of the stacking of predictive densities algorithm.

APPENDIX K. RECOVER EXPECTED z AND LOG POINT-WISE PREDICTIVE DENSITY FOR MCMC SAMPLING

The package *spBayes* doesn't record the posterior samples of the latent process $z(s)$. In this subsection, we illustrate how to recover the expected $z(s)$ for both observed and unobserved location and compute MLPD for the simulation studies based on the outputs returned by *spLM*. To achieve our goal, we need to recover the posterior samples of $z(s)$ on all locations given the recorded MCMC samples of parameters $\Phi = \{\phi, \nu\}$, σ^2, τ^2 and β . Denote $z(s)$ on observed and unobserved locations as z_o and z_u , respectively, and denote $z(s)$ on all locations as z^* . Based on (2.2),

$$\begin{aligned} p\left(\underbrace{\begin{bmatrix} z_o \\ z_u \end{bmatrix}}_{z^*} \mid y, \beta, \sigma^2, \Phi\right) &\propto \mathcal{N}(y \mid X\beta + \begin{bmatrix} I_n & 0 \end{bmatrix} \begin{bmatrix} z_o \\ z_u \end{bmatrix}, \tau^2 I) \times \mathcal{N}\left(\begin{bmatrix} z_o \\ z_u \end{bmatrix} \mid 0, \sigma^2 R_\Phi(\chi^*)\right) \\ &\propto \exp\left[-\frac{1}{2} \left\{ \tau^{-2} \left(\begin{bmatrix} I_n & 0 \end{bmatrix} z^* - (y - X\beta) \right)^\top \left(\begin{bmatrix} I_n & 0 \end{bmatrix} z^* - (y - X\beta) \right) + z^{*\top} \sigma^{-2} R_\Phi^{-1}(\chi^*) z^* \right\}\right] \\ &\propto \exp\left[-\frac{1}{2} \left\{ z^{*\top} \left(\sigma^{-2} R_\Phi^{-1}(\chi^*) + \begin{bmatrix} \tau^{-2} I_n & 0 \\ 0 & 0 \end{bmatrix} \right) z^* \right\}\right] \\ &\quad \exp\left[\frac{-1}{2} \left\{ -z^{*\top} \begin{bmatrix} (y - X\beta)/\tau^2 \\ 0 \end{bmatrix} - \begin{bmatrix} (y - X\beta)^\top/\tau^2 & 0 \end{bmatrix} z^* \right\}\right] \\ &\propto \mathcal{N}(z^* \mid M_z^* m_z^*, M_z^*), \end{aligned}$$

where χ^* combines the observed and unobserved location sets and

$$M_z^* = \left(\sigma^{-2} R_\Phi^{-1}(\chi^*) + \begin{bmatrix} \tau^{-2} I_n & 0 \\ 0 & 0 \end{bmatrix} \right)^{-1}, \quad m_z^* = \begin{bmatrix} (y - X\beta)/\tau^2 \\ 0 \end{bmatrix}.$$

Let $\{\beta^{(j)}, \sigma^{2(j)}, \tau^{2(j)}, \phi^{(j)}, \nu^{(j)}\}$ for $j = 1, \dots, J$ denote the recorded MCMC samples. We generate posterior samples for z^* using the above full conditional posterior distribution for each iteration j and then compute the average as the expected z^* . We further compute the

LPD of $y(s)$ any held out location s by

$$\begin{aligned}
lp(s) &= \log \int_{\beta, z(s), \tau^2} p(y(s) | \beta, z(s), \tau^2) p(\beta, z(s), \tau^2 | y) d\beta dz(s) d\tau^2 \\
&= \log \left\{ \frac{1}{J} \sum_{j=1}^J p(y(s) | \beta^{(j)}, z(s)^{(j)}, \tau^{2(j)}) \right\} \\
&= \log \left\{ \frac{1}{J} \sum_{j=1}^J \mathcal{N}(y(s) | x(s)^\top \beta^{(j)} + z(s)^{(j)}, \tau^{2(j)}) \right\}
\end{aligned}$$

APPENDIX L. COMPUTE THE STACKING WEIGHTS FOR STACKING OF MEANS (IN R CODE)

Let us format the expected outcome $\{\mathbb{E}(y[k] | y[-k], \phi, \nu, \delta^2)\}_{(\phi, \nu, \delta^2) \in G_{all}}^{k=1, \dots, K}$ computed in Algorithm 2 by an $N \times G$ matrix \hat{Y} . Each column of \hat{Y} stores the expected outcome $\{\mathbb{E}(y[k] | y[-k], \phi, \nu, \delta^2)\}_{k=1, \dots, K}$ for each candidate model, and it shares the same order of observed locations as the outcome y . Let $w = (w_1, w_2, \dots, w_G)^\top$ be the stacking weights, we need to find the weights that satisfy

$$\operatorname{argmin}_w \{(y - \hat{Y}w)^\top (y - \hat{Y}w)\},$$

under the constrain $\sum_g w_g = 1$. Now we modify it into a quadratic programming (QP) problem.

$$\begin{aligned}
&(y - \hat{Y}w)^\top (y - \hat{Y}w) \\
&= \left\{ (y - \sum_g w_g \hat{Y}_G) - \sum_g w_g (\hat{Y}_g - \hat{Y}_G) \right\}^\top \left\{ (y - \sum_g w_g \hat{Y}_G) - \sum_g w_g (\hat{Y}_g - \hat{Y}_G) \right\} \\
&= (\tilde{y} - \tilde{Y}\tilde{w})^\top (\tilde{y} - \tilde{Y}\tilde{w})
\end{aligned}$$

where $\tilde{y} = y - \hat{Y}_G$, $\tilde{Y} = [(\hat{Y}_1 - \hat{Y}_G) : \dots : (\hat{Y}_{G-1} - \hat{Y}_G)]$, and $\tilde{w} = (w_1, \dots, w_{G-1})^\top$. And the QP problem has constrains $-\sum_{g=1}^{G-1} w_g \geq -1$ and $w_g \geq 0$ for $g = 1, \dots, G-1$.

APPENDIX M. FIGURES FOR SIMULATION STUDIES

M.1. Distributions of the counts of nonzero weights for simulation 1 and 2. See Figure 10.

M.2. Interpolated maps for the simulation studies. See Figures 11, 12, 13 and 14.

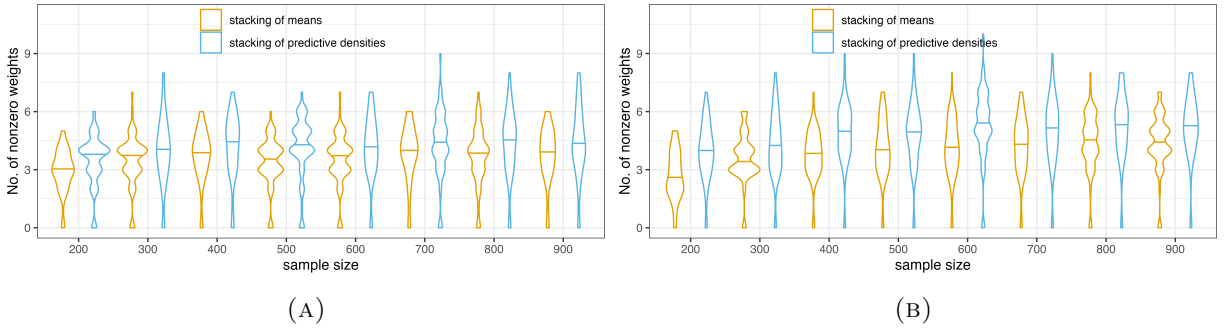


FIGURE 10. Distributions of the counts of nonzero weights in the first (a) and the second (b) simulation. The distribution of the counts are described through violin plots whose horizontal lines indicate the medians.

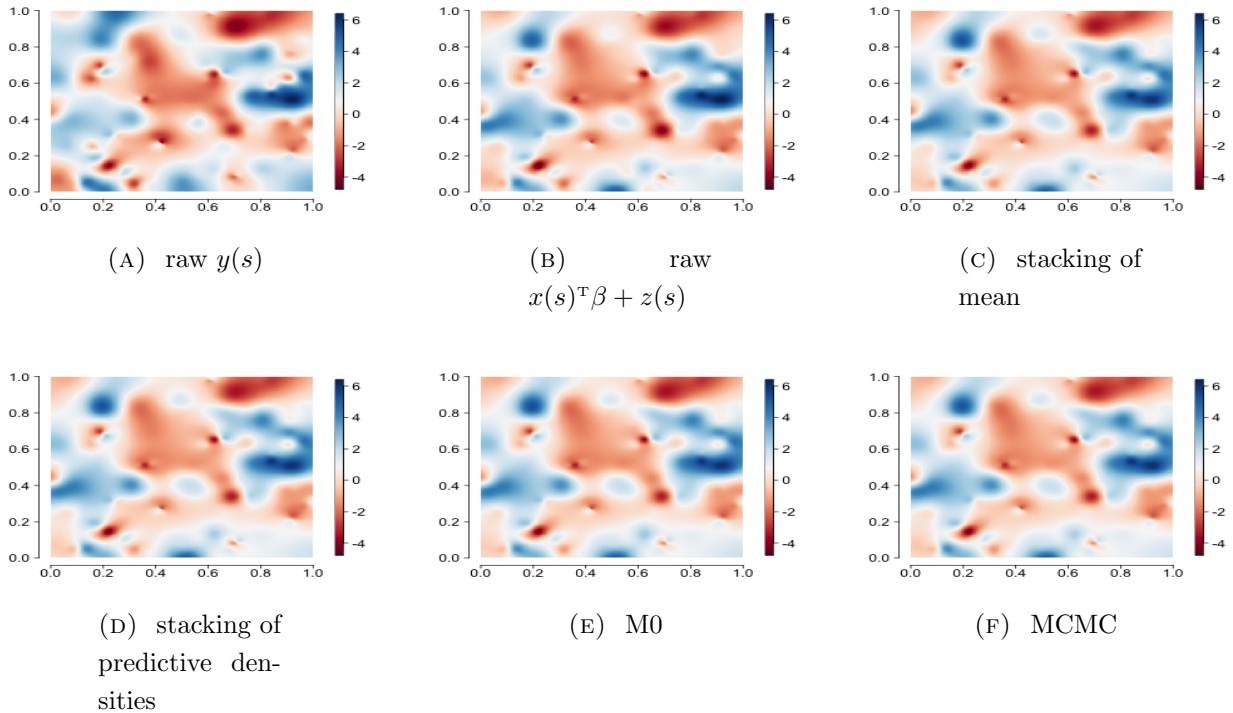


FIGURE 11. Interpolated maps of (a) the response $y(s)$, (b) the denoised response $x(s)\beta + z(s)$ and (c-f) the expected $y(s)$ on the $n_h = 100$ held out locations generated by all competing algorithms for the example with 800 observations from the first simulation.

M.3. Inference of prefixed hyper-parameters. A limitation of stacking, compared to full Bayesian inference (e.g., using MCMC), is that it does not provide inference for the prefixed hyper-parameters. If we treat the grid of the candidate values for the hyper-parameters

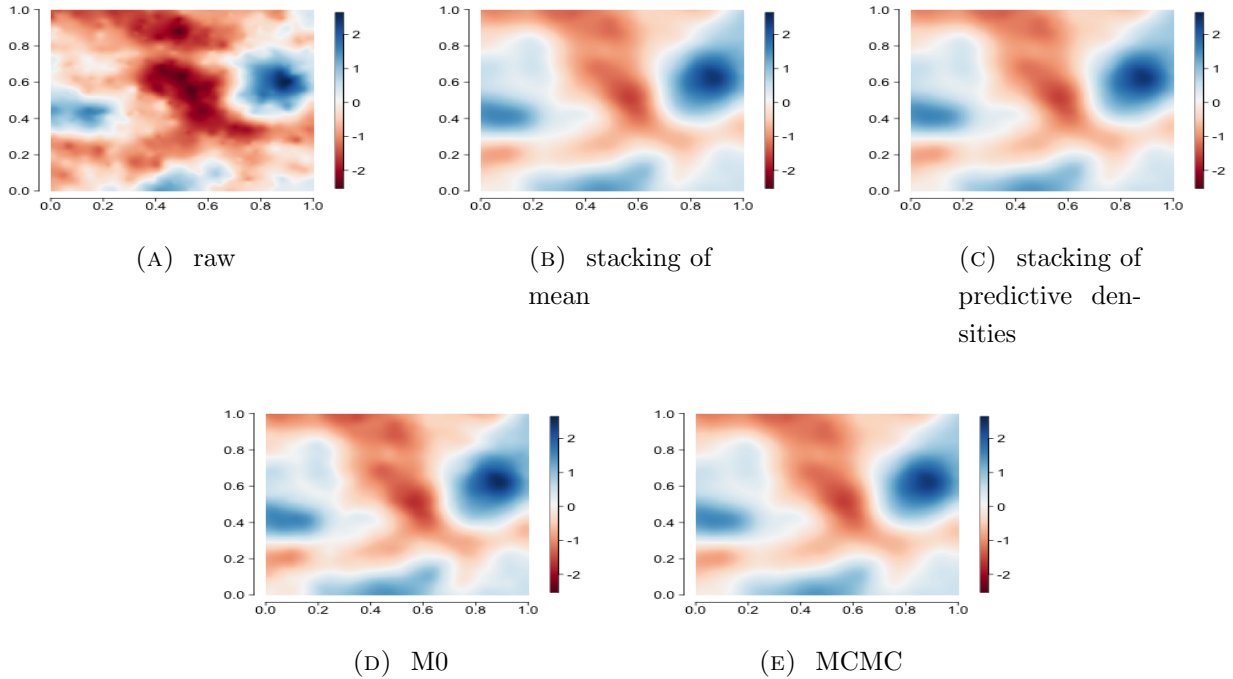


FIGURE 12. Interpolated maps of (a) the latent process $z(s)$ and (b-g) the expected $z(s)$ on all $n = 900$ sampled locations generated by all competing algorithms for the example from the first simulation. The $n = 900$ locations include both observed and unobserved locations

in our stacking algorithms as a discrete uniform prior, then, intuitively, one might be tempted to treat the stacking weights as probability masses on the support of the hyper-parameters. This intuition, however, is incorrect. Figure 15 compares the point estimates of ϕ based on stacking for the simulation studies. It is clear that stacking of means yields unstable estimates. Stacking of predictive densities has a smaller variance, but the bias can be large. Also, since ϕ is not identifiable, we observe that the posterior interval estimates for ϕ inferred from MCMC algorithms are wide, showing that the inference for ϕ is relatively unstable for all candidate algorithms in this simulation study. Figures 16 and 17 presents similar comparisons for the other two hyper-parameters.

M.4. Plots for the simulation study in Section 5.4. See Figures 18, 19 and 20.

APPENDIX N. PLOTS FOR AOD PREDICTION ANALYSIS

See Figures 21 and 22.

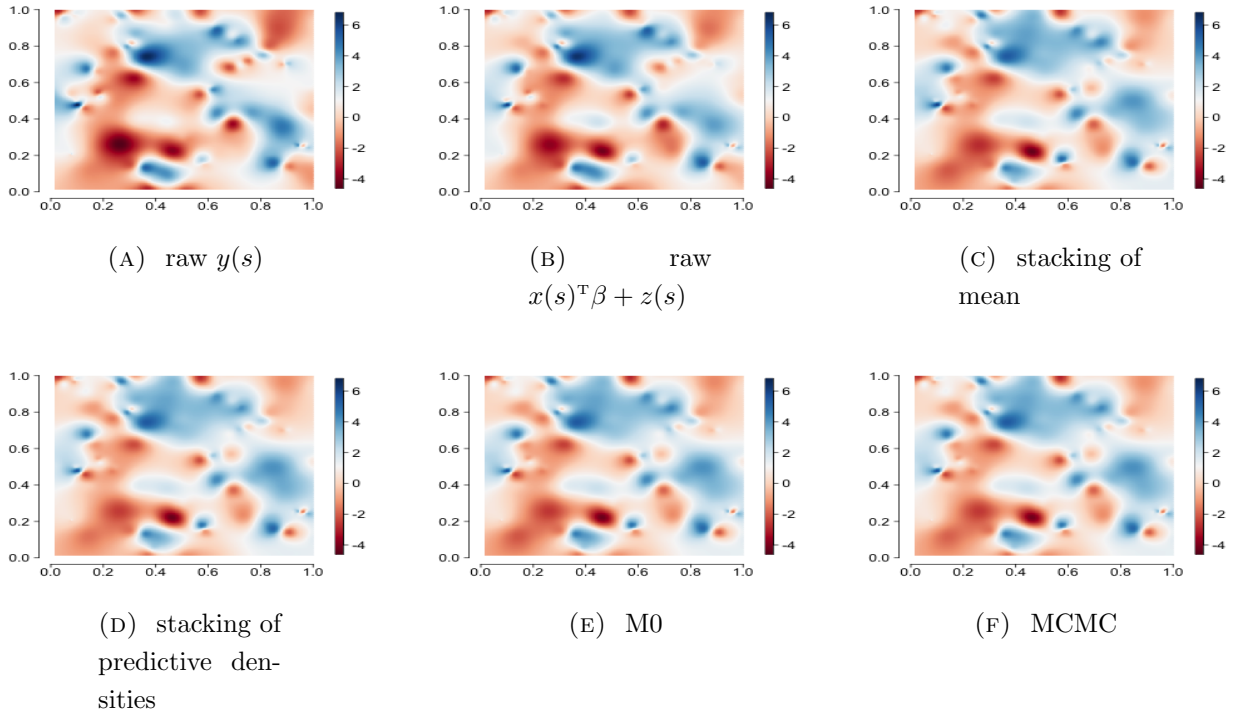


FIGURE 13. Interpolated maps of (a) the response $y(s)$, (b) the denoised response $x(s)\beta + z(s)$ and (c-f) the expected $y(s)$ on the $n_h = 100$ held out locations generated by all competing algorithms for the example with 400 observations from the second simulation.

Algorithm 3 Stacking of predictive densities (Monte Carlo Version)

- 1: **Input:** X, y, χ : Design matrix, outcome and location set; $\mu_\beta, V_\beta, a_\sigma, b_\sigma$: Prior parameters; $G_\phi, G_\nu, G_{\delta^2}$: Grids of ϕ, ν, δ^2 ; K Number of folders; J : number of samples for log point-wise predictive density estimation
 - 2: **Output:** $w = \{w_{\phi, \nu, \delta^2}\}_{(\phi, \nu, \delta^2) \in G_{all}}$: Stacking weights; G_{all} : Grid spanned by $G_\phi, G_\nu, G_{\delta^2}$
 - 3: **function** SPSTACKINGMC($X, y, \chi, \mu_\beta, V_\beta, a_\sigma, b_\sigma, G_\phi, G_\nu, G_{\delta^2}, \phi, \nu, \delta^2, K, J$)
 - 4: Compute $X_{\text{prod}}^{(k)} = X^T[-k]X[-k]$, $X_y^{(k)} = X^T[-k]y[-k]$, $\|y[-k]\|^2 = y^T[-k]y[-k]$ and record the number of observations n_k in fold k for $k = 1, \dots, K$, where $X[-k]$ $y[-k]$ denotes the predictors and response for observations not in fold k
 - 5: **for** $\Phi = \{\phi, \nu\}$ in grid expanded by G_ϕ and G_ν **do**
 - 6: **for** $k = 1$ to K **do**
 - 7: Calculate $R_\Phi^{-1}(\chi[-k]) = (R_\Phi^{-1}(s, s'))_{s, s' \in \chi[-k]}$ $\mathcal{O}(n^3)$
 - 8: Store $J_\Phi(\chi[k], \chi[-k]) = (R_\Phi(s, s'))_{s \in \chi[k], s' \in \chi[-k]}$
 - 9: **for** δ^2 in G_δ^2 **do**
 - 10: Compute the Cholesky decomposition L_* of
 - 11:
$$M_*^{-1} = L_* L_*^T = \begin{bmatrix} \delta^{-2} X_{\text{prod}}^{(k)} + V_\beta^{-1} & \delta^{-2} X^T[-k] \\ \delta^{-2} X[-k] & R_\Phi^{-1}(\chi[-k]) + \delta^{-2} I_{n-n_k} \end{bmatrix}$$
 $\mathcal{O}(n^3)$
 - 12: Compute $x = m_* = \begin{bmatrix} V_\beta^{-1} \mu_\beta + \delta^{-2} X_y^{(k)} \\ \delta^{-2} y[-k] \end{bmatrix}$
 - 13: Solve $L_* u = x$ with forward solver
 - 14: Compute $b_* = b_\sigma + 0.5(\delta^{-2} \|y[-k]\|^2 + \mu_\beta^T V_\beta^{-1} \mu_\beta - u^T u)$ and
 - 15: $a_* = a_\sigma + 0.5(N - n_k)$
 - 16: Generate $\sigma^{2(1)}, \dots, \sigma^{2(J)} \sim \text{Inverse-Gamma}(a_*, b_*)$
 - 17: Generate $\gamma^{(j)} \sim \text{N}(M_* m_*, \sigma^{2(j)} M_*)$ by taking $v^{(j)} \sim \text{N}(0, \sigma^{2(j)} I_{n-n_k+p})$ and
 - 18: computing $\gamma^{(j)} = L_*^{-T}(v^{(j)} + u)$ for $j = 1, \dots, J$
 - 19: Generate the posterior samples of the expected outcome on locations in
 - 20: fold k : $\hat{y}_{(\phi, \nu, \delta^2)}^{(k, j)} = X[k] \gamma_\beta^{(j)} + J_\Phi(\chi[k], \chi[-k]) \cdot R_\Phi^{-1}(\chi[-k]) \gamma_z^{(j)}$, $j = 1, \dots, J$
 - 21: **for** $s \in S[k]$ **do**
 - 22: Compute the posterior samples of the log-density of observation $y(s)$
 - 23: at location s , $p_{(\phi, \nu, \delta^2)}(y(s) | \sigma^{2(j)}, \gamma^{(j)})$ by taking the density of
 - 24: $\text{N}(\hat{y}_{(\phi, \nu, \delta^2)}^{(k, j)}(s), \delta^2 \sigma^{2(j)})$ at $y(s)$ for $j = 1, \dots, J$ (J.1)
 - 25: Compute the expected log point-wise predictive density of $y(s)$ at loca-
 - 26: tion s , by $lp_{(\phi, \nu, \delta^2)}(s) = \log \left[\frac{1}{J} \sum_{j=1}^J p_{(\phi, \nu, \delta^2)}(y(s) | \sigma^{2(j)}, \gamma^{(j)}) \right]$ (J.2)
 - 27: Solve convex optimization problem: Under constrains $\sum_{(\phi, \nu, \delta^2) \in G_{all}} w_{(\phi, \nu, \delta^2)} = 1$ and $w_{(\phi, \nu, \delta^2)} > 0$ maximize $\sum_{s \in \chi} \log(\sum_{(\phi, \nu, \delta^2) \in G_{all}} \exp \{lp_{(\phi, \nu, \delta^2)}(s)\} * w_{(\phi, \nu, \delta^2)})$
 - 28: **return** $\{w, G_{all}\}$,
-

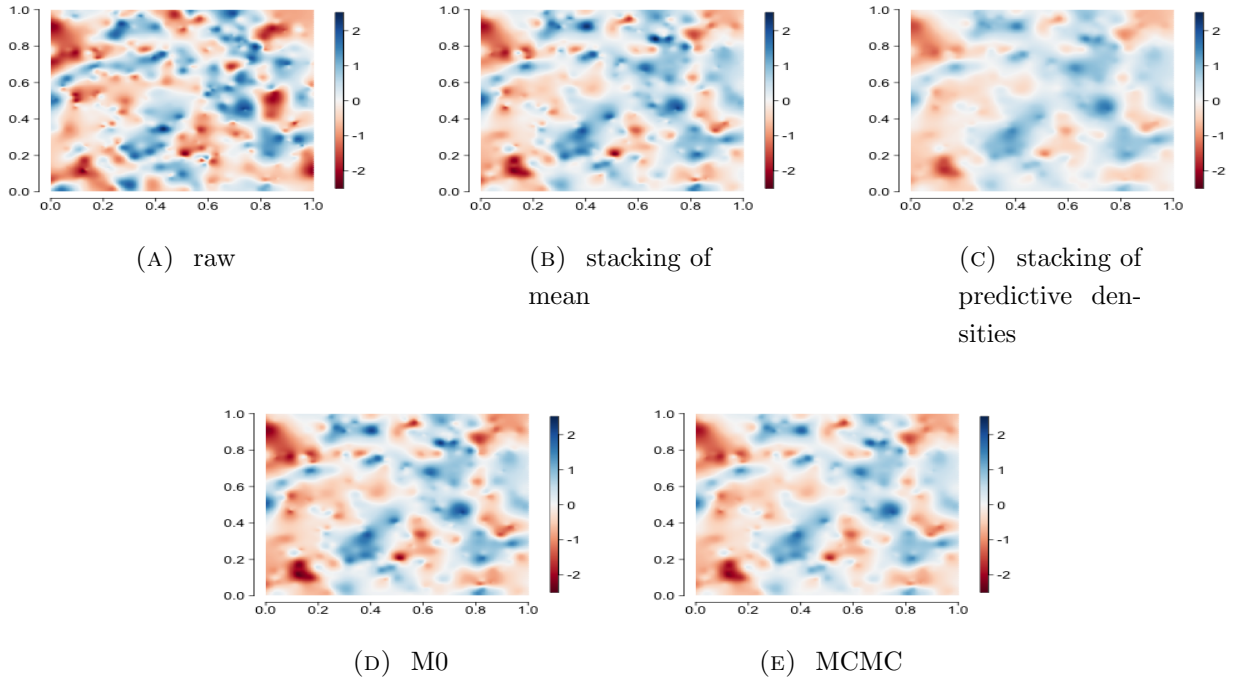


FIGURE 14. Interpolated maps of (a) the latent process $z(s)$ and (b-g) the expected $z(s)$ on all $n = 500$ sampled locations generated by all competing algorithms for the example from the second simulation. The $n = 500$ locations include both observed and unobserved locations

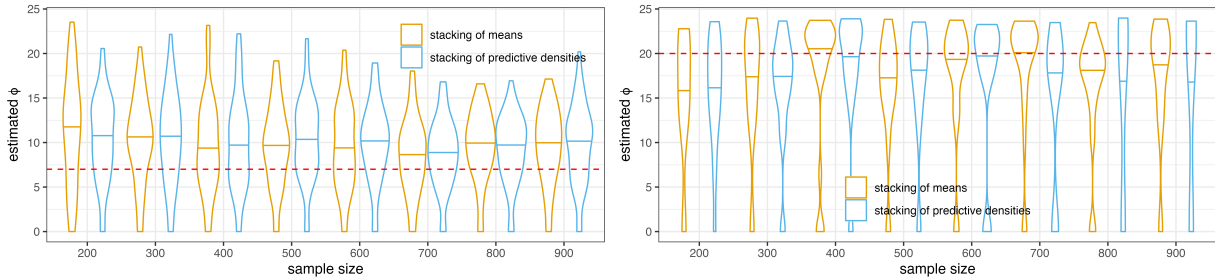
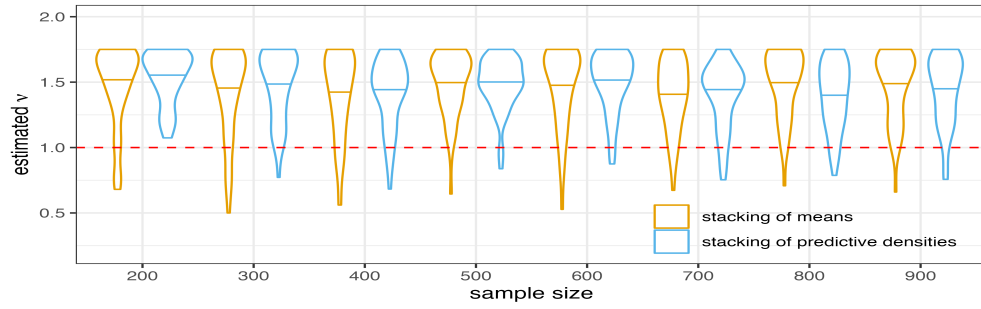
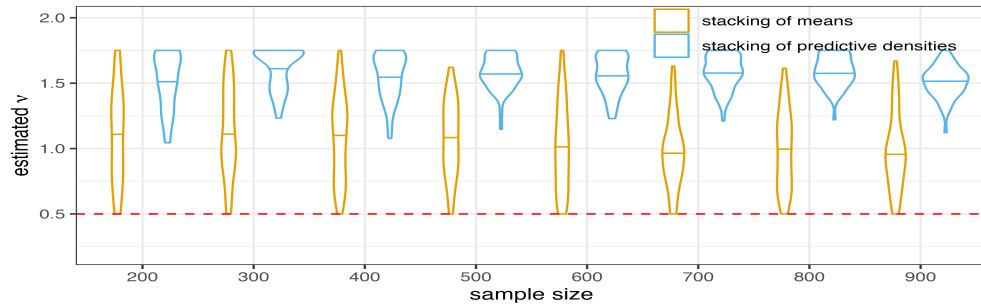


FIGURE 15. Distributions of the estimated ϕ in the first (left panel) and the second (right panel) simulation. The distributions are described by violin plots whose horizontal lines indicate the medians. The red dashed horizontal line indicates the actual value of ϕ

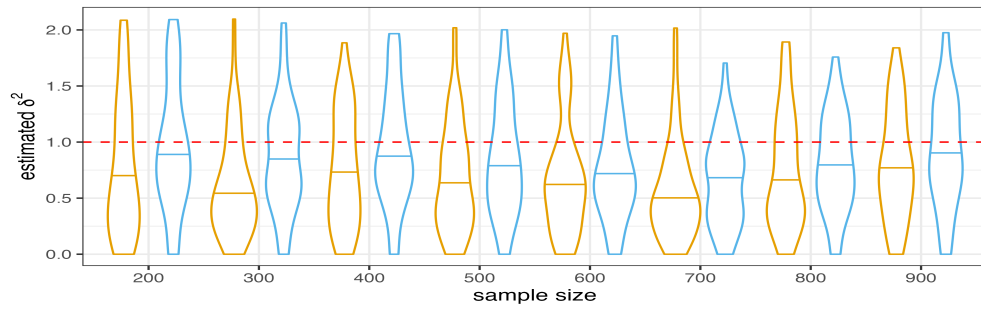


(A)

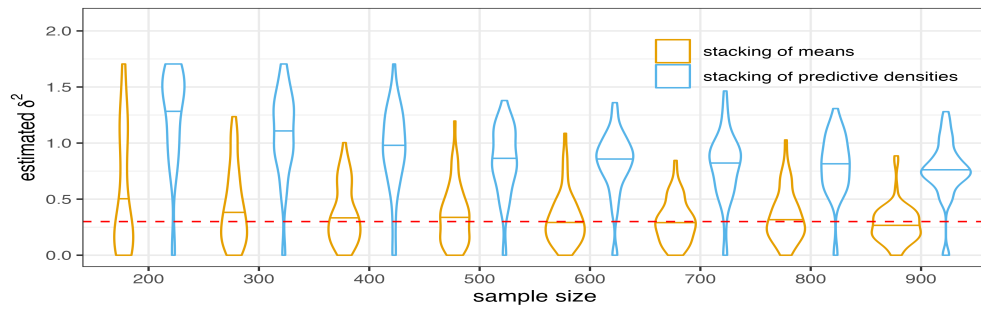


(B)

FIGURE 16. Distributions of the estimated ν in the first (a) and the second (b) simulation. The distribution of the counts are described through violin plots whose horizontal lines indicate the medians. The red dashed horizontal line indicates the actual value of ν



(A)



(B)

FIGURE 17. Distributions of the estimated δ^2 in the first (a) and the second (b) simulation. The distribution of the counts are described through violin plots whose horizontal lines indicate the medians. The red dashed horizontal line indicates the actual value of δ^2

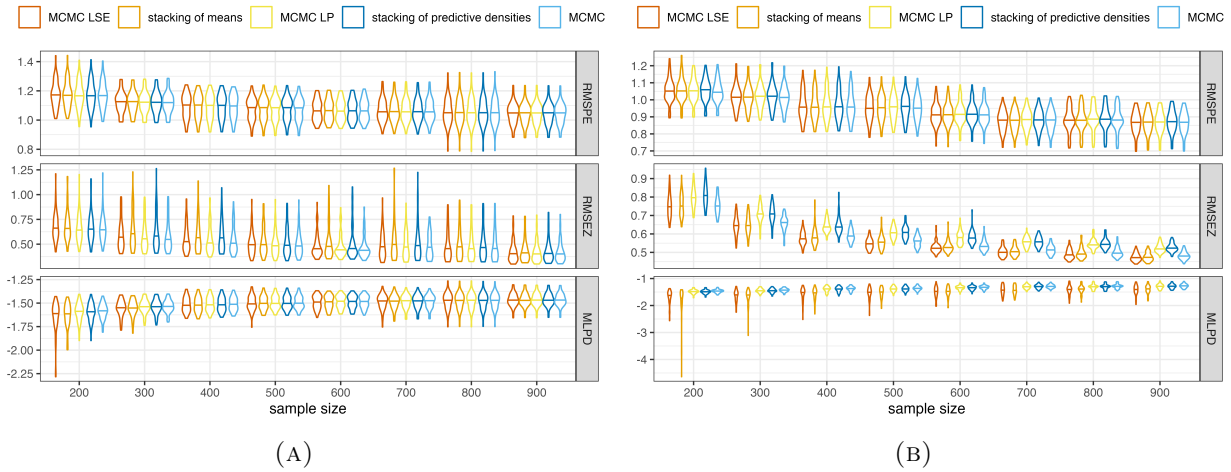


FIGURE 18. *Distributions of the diagnostic metrics for prediction performance for the first simulation (a) and the second simulation (b). Label ‘MCMC LSE’ and ‘MCMC LP’ denote stacking of mean and stacking of predictive densities using ϕ , ν , δ^2 sampled through MCMC, respectively. Each distribution is depicted through a violin plot. The horizontal line in each violin plot indicates the median.*

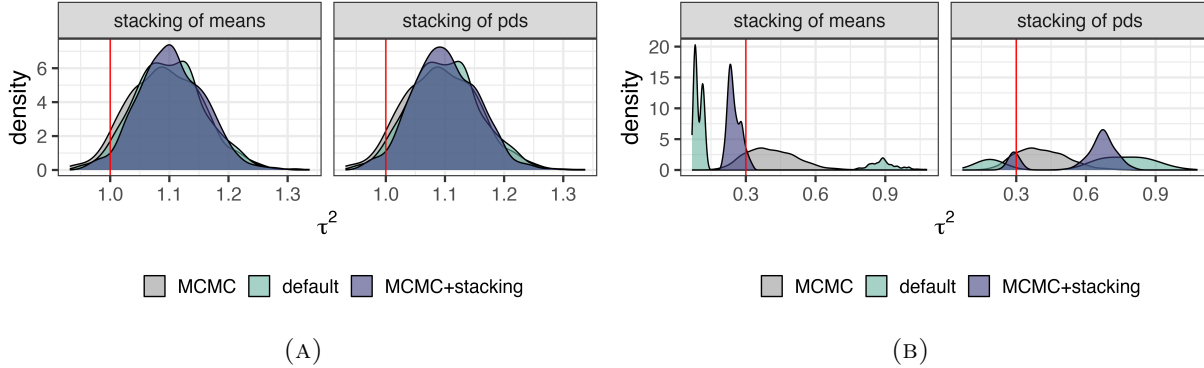


FIGURE 19. *Densities of τ^2 for the example with 800 observations from simulation 1 (a) and the example with 400 observations from simulation 2 (b). Vertical red lines indicate the actual τ^2 values. Grey densities represent MCMC-recovered posterior distributions of τ^2 . ‘Default’ and ‘MCMC+Stacking’ show stacking results using two methods for selecting ϕ , ν , δ^2 candidates. Left panel: stacking of means. Right panel: stacking of predictive densities*

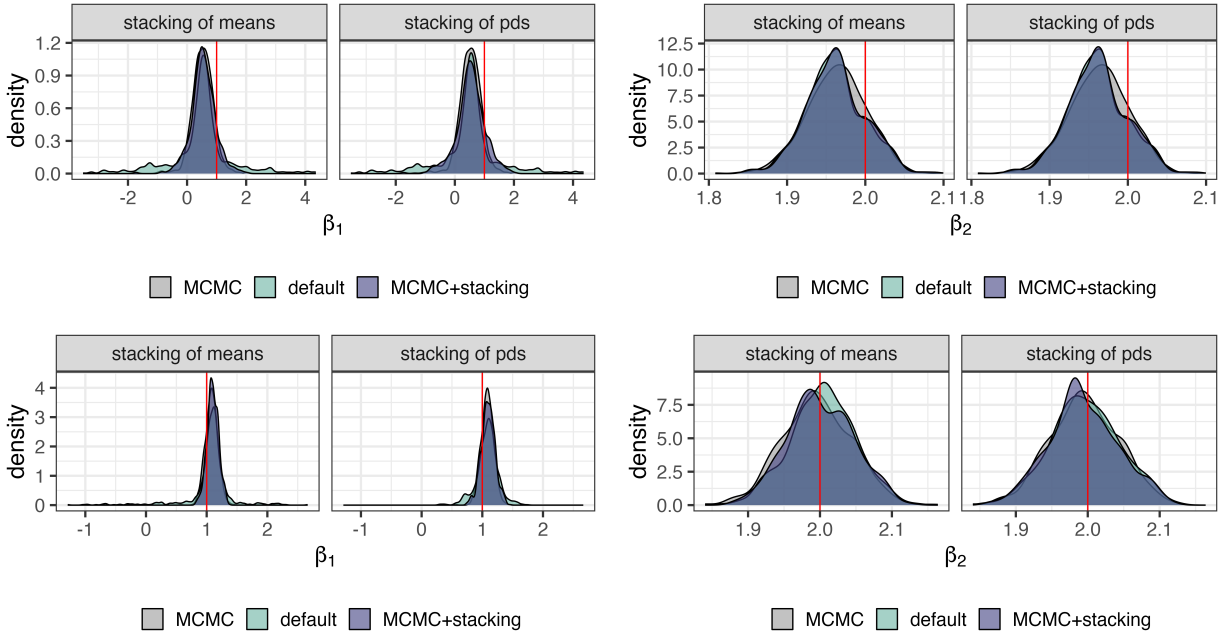


FIGURE 20. Densities of β_1 (left column) and β_2 (right column) for the example with 800 observations from simulation 1 (upper row) and the example with 400 observations from simulation 2 (lower row). Vertical red lines indicate the actual values. Grey densities represent MCMC-recovered posterior distributions. 'Default' and 'MCMC+Stacking' show stacking results using two methods for selecting ϕ, ν, δ^2 candidates. Left panel: stacking of means. Right panel: stacking of predictive densities

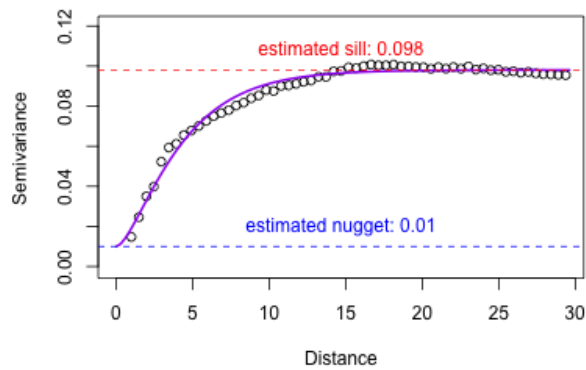


FIGURE 21. Semivariogram of the residuals from AOD linear regression model

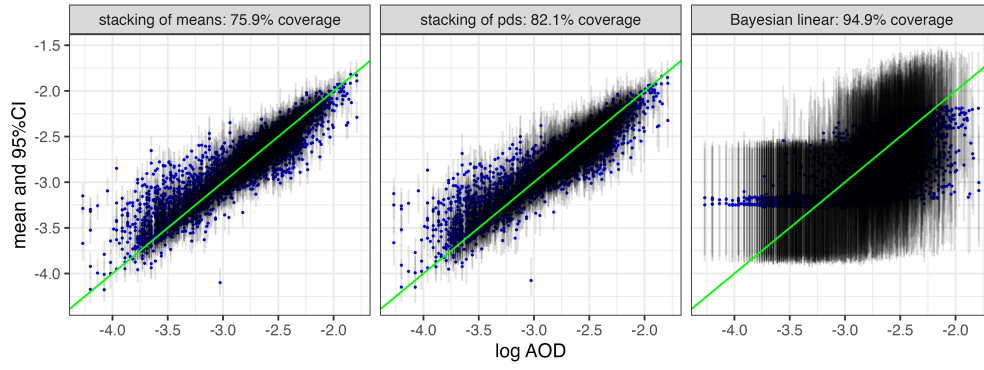


FIGURE 22. Scatterplots for log of interpolated and testing data AOD with 95% credible intervals. Solid green line denotes the 45-degree line. Titles include 95%CI coverage.